Dating the detachment fault system of the Ruby Mountains, Nevada: Significance for the kinematics of low-angle normal faults

Samuel H. Haines[1,2] and Ben A. van der Pluijm[1]

Received 9 June 2009; revised 10 March 2010; accepted 26 April 2010; published 21 August 2010.

[1] The mechanics of low-angle normal faulting and metamorphic core complexes continue to be a subject of debate. We investigate the conditions, timing, and kinematics of slip in the late, upper-crustal stages of core complex evolution of the Ruby Mountains detachment fault at the well-exposed Secret Pass locality with an X-ray diffraction (XRD) and Ar-Ar study of clay gouge samples from three separate faults, two from the low-angle detachment system and one from a high-angle normal fault that soles into the main detachment fault system. XRD analysis and modeling of XRD analysis show that authigenic illite-rich illite/smectite (I/S) in gouge at Secret Pass is distinguishable from clay phases in hanging wall rocks because the I/S in the gouges contains only one-water layer as opposed to the more common two-water I/S phases found in both the hanging wall and footwall. Ar-Ar ages for the monomineralic one-water I/S found in the hanging wall high-angle fault, the main detachment, and a low-angle normal fault structurally above the main detachment are 11.6 ± 0.1 Ma, 12.3 ± 0.1 Ma, and <13.8 ± 0.2 Ma, respectively. The not-quite-flat Ar-Ar spectra indicate the gouge illites grew over some interval of time and not in discrete events. The nearly overlapping ages indicate that gouge formation and thus the last major period of activity on the detachment were at 11–13 Ma and were active coevally as part of a kinematically linked fault system with the main detachment active at dips <45° and possibly as low as 22°.
Citation: Haines, S. H., and B. A. van der Pluijm (2010), Dating the detachment fault system of the Ruby Mountains, Nevada: Significance for the kinematics of low-angle normal faults, *Tectonics*, *29*, TC4028, doi:10.1029/2009TC002552.

1. Introduction

[2] The evolution of metamorphic core complexes, particularly in the elastofrictional regime, remains one of the major controversies in structural geology. Metamorphic core complexes are particularly common in the eastern Basin and Range province of North America, extending from southern British Columbia to northwest Mexico, recording large-magnitude extension [e.g., *Coney*, 1980; *Snoke*, 1980]. Most core complexes have a gently dipping dome-shaped metamorphic "core" of midcrustal rocks, which are topped by a "carapace" of mylonitic quartzo-feldspathic rocks, quartzites or mylonitic carbonate rocks. The mylonites are overlain and cut by brittle fault rocks (breccias, cataclasites, and clay-rich gouges), collectively recording a characteristic crystal-plastic-to-frictional strain history. The hanging wall blocks are often un- or weakly metamorphosed and are cut by high-angle normal faults that sole into a main detachment surface. Core complex detachments have accommodated large horizontal displacements, on the order of tens of kilometers, and are responsible for the removal of a significant portion of the crustal section, in the range of 5–15 km [*Axen*, 2004].

[3] Core complex detachments are controversial, because many detachment fault surfaces have dips <30° [*John*, 1987]. Such low dips of faults contradict our understanding of rock mechanics as normal faults should not form in the elastofrictional regime (typically <300°C for most silicate rocks) at such low dips [*Anderson*, 1942; *Scholz*, 2002], assuming a vertical maximum compressive stress, typical values of sliding friction for rock (μ = 0.65–0.8) [*Byerlee*, 1978] and mostly isotropic material. Furthermore, there is considerable debate about the potential for seismicity on low-angle normal faults (LANFs) [e.g., *Collettini and Sibson*, 2001]. Although several studies have noted a lack of evidence for focal mechanisms on LANF planes [*Jackson*, 1987; *Jackson and White*, 1989; *Wernicke*, 1995; *Collettini and Sibson*, 2001], recent work has documented that at least some of these structures generate seismicity [*Abers et al.*, 1997; *Chiaraluce et al.*, 2007]. The seismological argument adds to the debate about the frictional strength of faults [e.g., *Byerlee*, 1978; *Rice*, 1992] as slip on detachment faults at dips <30° would require low apparent friction compared to laboratory values.

[4] Dating the deformation related to the onset of exhumation of a core complex in the plastic regime is relatively straightforward [e.g., *McGrew and Snee*, 1994; *Vanderhaeghe et al.*, 2003], but dating the stages of brittle deformation, critical to understanding the kinematics of core complex evolution, is more difficult. Activity on brittle faults at core complexes has traditionally been dated by "bracketing," dating events that preceded and followed the faulting [e.g., *Miller and John*, 1999; *Wong and Gans*, 2003] or by inferences from thermochronometer ages [e.g., *Miller et al.*, 1999; *Carter et al.*, 2006]. Frequently, the constraints placed on the timing of brittle deformation in core complex detachments are not well defined when compared to the earlier evolution of these structures.

[1]Department of Geological Sciences, University of Michigan, Ann Arbor, Michigan, USA.
[2]Department of Geosciences, Pennsylvania State University, University Park, Pennsylvania, USA.

0278-7407/10/2009TC002552

[5] We directly determine the age of brittle deformation on multiple faults in the Ruby Mountains detachment fault system by dating authigenic illite growing in clay gouge. In addition, dating gouges from multiple faults in the detachment system places important constraints on the kinematics and evolution of detachment fault systems. As the high-angle normal faults in the hanging wall blocks have a more "typical" (e.g., listric) geometry and can reasonably inferred to have formed under a vertical maximum compressive stress regime, their age relations to the main detachment are key in determining whether the main low-angle detachment was active at the same time and presumably the same stress field. If the main detachment is older than high-angle faults, then the main detachment could have formed earlier, at a high angle, and been subsequently passively rotated to a low angle. This possible rotation to lower dips occurs either as part of the passage of a "rolling hinge" in a strict sense [e.g., *Wernicke and Axen*, 1988; *Buck*, 1988], where active slip occurs only on the high-angle portion of a detachment system that becomes inactive as it is rotated by the passage of a "rolling hinge" or as part of a normal fault system that initiated at high angles but gradually rotated to lower dips during progressive extension [e.g., *Proffett*, 1977; *Gans et al.*, 1985; *Wong and Gans*, 2008].

[6] Establishing a kinematic link between activity on the main detachment and the higher-angle normal faults that sole into the main detachment has been demonstrated at uppermost levels of the crust (upper 3 km) [e.g., *Cichanski*, 2000; *Hayman et al.*, 2003], but extrapolating this kinematic linkage to deeper crustal levels, such as those at which authigenic clay-rich gouges form, has not previously been demonstrated. Establishing a kinematic link between high-angle normal faults and the main detachment can also place constraints on the dip of the main detachment at the time of gouge formation. We aim to demonstrate that the kinematic link between the main detachment and higher-angle faults that sole into the main detachment suggested from results in the shallow crust is also valid to the depth at which clay gouges form and thus potentially the case for upper-crustal detachment systems as a whole.

[7] Previous evidence of a kinematic linkage between high-angle normal faults in the upper plate and the main detachment has depended on exceptional field exposures with datable strata at very young detachments. Until recently, the lack of a reliable method to directly date clay gouges has prohibited linking coeval activity on both the main detachment and higher-angle normal faults in other detachment systems where field relations are less clear. Some core-complex hanging walls lack volcanogenic strata dateable by conventional means, while others lack the appropriate phyllosilicate-rich wall rocks to generate clay-rich fault gouge amenable to dating. However, the Secret Pass area of the Ruby-East Humboldt metamorphic core complex in northeastern Nevada exposes a hanging wall normal fault that has well-developed clay gouge that is suitable for dating by Ar-Ar methods, in addition to gouge-rich exposures of the main detachment fault. The age of clay gouge from the hanging wall normal fault can then be compared with the age of gouge from the main detachment to elucidate the temporal relationship of these faults that currently have contrasting high and low dips.

2. Clay Mineralogy Terminology and Fault Gouge Dating

2.1. Clay Mineralogy Terminology

2.1.1. Mixed Layer Clays

[8] The terminology used to describe clay minerals, particularly clay phases that consist of interlayers of more than one clay mineral (e.g., interlayered illite-smectite) is complex and requires a brief treatment here. To fully describe a mixed layer clay mineral, three properties of the mixed layer phase must be described: (1) the two types of layers involved, (2) the relative proportions of each layer, and (3) the stacking sequence of the two layers (ordered, semiordered, or random). The types of the two layers are established from multiple X-ray diffraction (XRD) analyses of the same material, typically before and after solvation with ethelyne glycol to hydrate "swelling" clays, smectites, and vermiculites. Smectites typically adsorb two layers of ethylene glycol upon solvation, expanding a 10 Å spacing between basal layers to a ~17 Å basal spacing, whereas vermiculite-like clays typically adsorb only one glycol layer, resulting in a smaller 14.4 Å basal *d* spacing. Illite that contains no interlayers of swelling phases retains a 10 Å basal spacing both before and after glycol solvation. The abundance of the swelling and nonswelling phase is identified from changes in the position of the basal 00*l* reflections, owing to the mixed layer phase containing a combination of 10 Å and either 14 Å or 17 Å layers. Whether the stacking of the two layer types is ordered (e.g., ISISISISIS) or random (e.g., SIIISISSIS) is ascertained from the presence or absence of higher-order reflections (e.g., a 27 Å peak at ~3° 2Θ on an XRD scan, caused by the regular interlayering of 10 and 17 Å phases). The ordering of interlayered clay minerals is referred to as "Reichweite" (*lit.* "reach-back," the chance, given layer A in a mixed layer mineral, of finding layer B next to it), and is conventionally expressed as a decimal between 0 and 1, so completely disordered illite/smectite (I/S) = R0, and completely ordered I/S = R1.

[9] The nature of illite-smectite phases has been linked to conditions of geologic formation. Mixed layer illite-smectite phases are commonly reported as a part of the transformation of smectite to illite that is widely observed in sedimentary basins [e.g., *Hower et al.*, 1976; *Ahn and Peacor*, 1986; *Freed and Peacor*, 1989a, 1989b; *Li et al.*, 1997; *Kim et al.*, 2004; *Huggett and Cuadros*, 2005; *Sandler and Saar*, 2007]. The transformation is generally agreed to be a prograde diagenetic series of reactions that begin at ~50°C and end below 150°C, with a general progression with depth of smectite → disordered smectite-rich I/S → illite-rich I/S → ordered (R1 and R3) illite-rich I/S → illite, although numerous other factors than temperature can effect the rate of these transformations [*Huang et al.*, 1993; *Essene and Peacor*, 1995] (see section 6). Mixed layer illite-smectites are also known from hydrothermal systems at a variety of temperatures from ~50°C to 280°C [*Lonker and Fitz Gerald*, 1990; *Junfeng et al.*, 1997].

2.1.2. Clay Polytypism

[10] Polytypism is a special case of polymorphism common to clay minerals and micas where the unit cell and density of the silicate structure remain unchanged, but the rotation of each individual silicate sheet with respect to the sheet above and below varies around the Z crystallographic axis. Polytypism of illite is of interest because it can be linked to environmental conditions of illite formation. Two distinct polytypes of illite are commonly found in nature, the $2M_1$, and the $1M_d$ polytypes, with three other known stacking sequences, the 1M, $2M_2$, and the 3T polytypes, that are only rarely observed [*Srodon and Eberl*, 1984]. The $2M_1$ polytype stacking sequence is common to high-temperature illites and muscovite and is characterized by regular 120° rotations of the 2:1 layers with a two-layer repeat, e.g., each second layer is oriented the same way. Experimental work indicates that the $2M_1$ polytype is the most stable illite polytype and is thought to form above 280°C [*Yoder and Eugster*, 1955; *Velde*, 1965; *Srodon and Eberl*, 1984], The $1M_d$ polytype stacking sequence is characterized by rotations of each silicate sheet in random multiples of 120° or more rarely 60° relative to the sheet above and below. The different rotation sequences of the silicate sheets are resolvable on an XRD pattern. $1M_d$ polytypes are thought to form at significantly lower temperatures, below approximately 200°C [*Velde*, 1965]. Studies in sedimentary basins have determined that the illite in sedimentary basins is nearly always a mixture of the $2M_1$ and $1M_d$ polytypes [*Grathoff et al.*, 2001]. The $2M_1$ polytype is typically found to be detrital material, while the $1M_d$ polytype is found primarily as very fine-grained material (e.g., pore-filling "hairy illites") and formed during diagenesis. The $1M_d$ polytype is the only polytype observed to form authigenically at temperatures below 200°C [*Grathhoff et al.*, 2001]. This observation is of key importance in considering the observed presence of $1M_d$ illite in fault gouge as it represents the brittle deformation realm. Smectite lacks multiple polytypic structures; all smectites are characterized by turbostratic (random) stacking of the silicate sheets, analogous to a pack of playing cards dropped onto a tabletop.

2.2. Fault Gouge Dating

[11] Dating fault gouge by the Ar-Ar or K-Ar methods requires the ability to compensate for the effect of the "contamination" of authigenic clays by detrital material, producing a mixed age. Early attempts to date fault gouges directly isolated a fine-grained fraction of illite (<2 μm) [*Lyons and Snellenburg*, 1970; *Kralik et al.*, 1987; *Damon and Shafiqullah*, 2006], erroneously assuming that these samples were free of detrital illite derived from the wall rocks. Dating of gouge thus tended to overestimate the age of faulting, as later work showed that some detrital material remains present in even very fine size fractions [*Pevear*, 1992; *Grathoff et al.*, 2001]. Subsequent applications of geochronological methods to date fault gouge [*van der Pluijm et al.*, 2001, 2006; *Ylagan et al.*, 2002; *Solum et al.*, 2005; *Haines and van der Pluijm*, 2008] have resolved the problem of detrital contamination by separating the gouge into several size fractions, each having a separate ratio of detrital and authigenic material, and iteratively modeling XRD patterns of the various size fractions to determine the percentage of authigenic and detrital material in each prior to vacuum-encapsulated Ar-Ar dating. Using an approach known as Illite Age Analysis, the percentage of detrital illite in each of the size fractions is plotted against its apparent Ar-Ar total gas ages and then extrapolated to 0% and 100% to find the end-member ages. Modeling programs NEWMOD© [*Reynolds and Reynolds*, 1996] and WILDFIRE© [*Reynolds*, 1993] are used to quantitatively determine the amounts of authigenic ($1M_d$) and detrital ($2M_1$) clays present in each size fractions of a gouge. Two clay mineral transformations lent themselves to this approach, the age of the illitization of illite/smectite [*van der Pluijm et al.*, 2001, 2006], and the growth of the authigenic, low-temperature $1M_d$ polytype of illite [*Solum et al.*, 2005; *Haines and van der Pluijm*, 2008]. While the percentage of illite in interlayered illite/smectite has been shown to increase in clay gouges relative to that found in the wall rock [*Vrolijk and van der Pluijm*, 1999], and the illitization of illite/smectite approach has been successfully used to date fault gouges, the illitization of illite/smectite approach is limited when illite (assumed to be detrital) occurs both in the wall rock and grows authigenically in the fault zone as the low-temperature $1M_d$ polytype [*Solum et al.*, 2005].

[12] Because some clay gouges can contain almost exclusively the authigenic $1M_d$ polytype of illite and either (1) lack sufficient $2M_1$ polytype to permit the conventional illite age analysis approach using the growth of authigenic $1M_d$ or (2) have a clay mineral assemblage that potentially contains more than two illitic phases and thus cannot be dated using the illitization of illite/smectite approach, we demonstrate that isolating, characterizing and dating a single fine fraction of the authigenic illite or illite-rich smectite alone can date authigenic clay growth in clay gouge. We model XRD patterns of the fine fraction material using NEWMOD© and WILDFIRE© to demonstrate that the fine fraction material is indeed monomineralic and contains only the $1M_d$ polytype. We demonstrate that the fine fraction illite in the gouge is distinct from authigenic fine fraction $1M_d$ illite that is observed in the wall rock. On the basis of NEWMOD© and WILDFIRE© modeling, we have been able to isolate essentially pure authigenic $1M_d$ illite in three fault gouges from the Ruby Mts detachment at Secret Pass and date them by the Ar-Ar method.

3. Field Area

[13] The Ruby Mountains are a well-exposed core complex in northeastern Nevada [*Howard*, 1980; *Snoke*, 1980] extending ~150 km along strike from SW to NE (Figure 1). The complex was exhumed along a large WNW dipping, 1–2 km thick shear zone that strikes along the NW side of the range. The detachment was active from the late Cretaceous to the Miocene [*Snoke and Lush*, 1984; *Dallmeyer et al.*, 1986; *Dokka et al.*, 1986; *Mueller and Snoke*, 1993; *McGrew and Snee*, 1994; *McGrew et al.*, 2000] and has a "typical" core complex plastic-to-brittle geometry. The time of onset of exhumation is somewhat unclear, as studies reported highly discordant hornblende $^{40}Ar/^{39}Ar$ ages ranging in age from

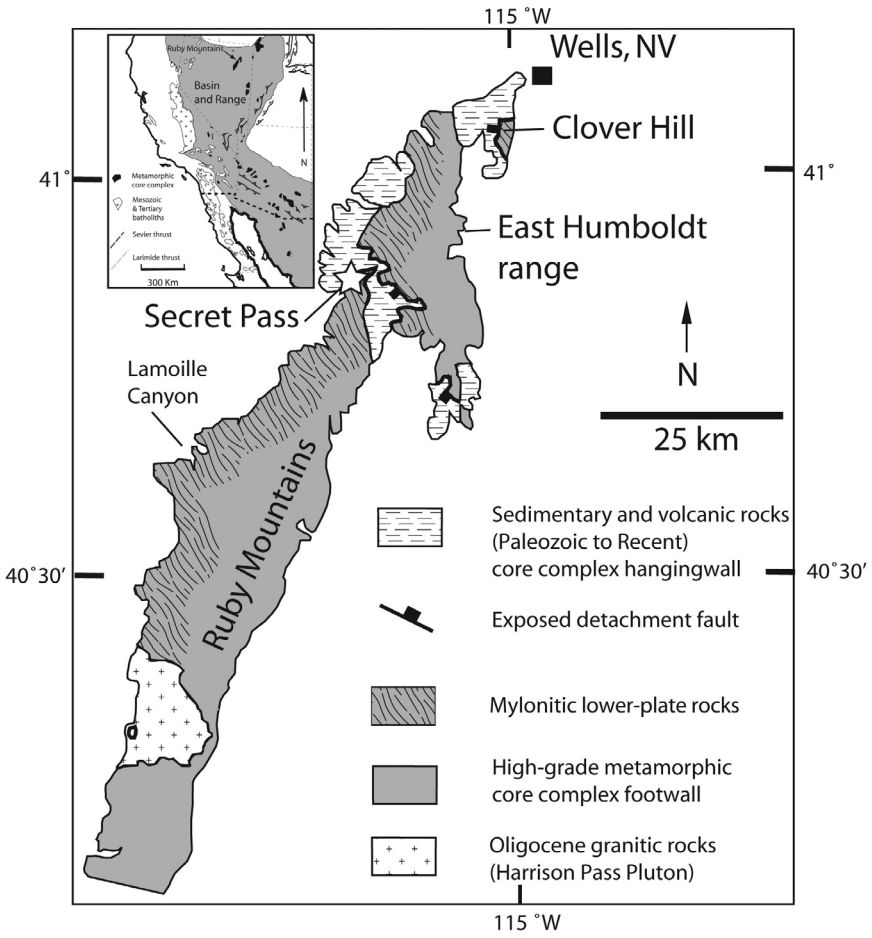

Figure 1. Generalized geologic map of the Ruby Mountains-East Humboldt Range in northeastern Nevada. Distribution of mylonitic lower-plate rocks is shown by lines. Redrawn from *Snoke and Lush* [1984]. Box shows area of Figure 2. Inset at top left: regional map showing major structural elements of the western US, redrawn from the work of *Coney* [1980].

Triassic to the upper Eocene [*Dallmeyer et al.*, 1986; *McGrew and Snee*, 1994], but exhumation probably was underway by the early Eocene in the eastern (updip) portion of the detachment with a crude trend of hornblende Ar-Ar younging toward the northwest, consistent with a SE-NW exhumation direction [*McGrew and Snee*, 1994]. Early deformation occurred at temperatures >500°C, evidenced by high-grade synkinematic mineral assemblages and dynamic recrystallization of both quartz and feldspar [*Snoke*, 1980; *Peters and Wickham*, 1994]. Exhumation to predominantly brittle conditions occurred rapidly during the late Oligocene and early Miocene, evidenced by 30–23 Ma $^{40}Ar/^{39}Ar$ cooling ages from muscovite and biotite [*Dallmeyer et al.*, 1986; *McGrew and Snee*, 1994], with a clearer trend of younger ages toward the northwest (downdip). The end of tectonic exhumation, however, is poorly constrained, as the age of Miocene sediments in the hanging wall is not well known. A rhyolite intercalated with the Miocene Humboldt Formation in the hanging wall at Secret Pass has been dated at 15.0 ± 1.6 Ma [*Snoke and Howard*, 1984], but age constraints on sediments below the lava are poor, and the field relationship of the detachment to the lava is unclear.

[14] The core complex detachment fault in the Ruby-East Humboldt Mountains is well exposed at two localities, at Secret Pass (between the Ruby Mountains and the East Humboldt range) and at Clover Hill at the NE corner of the East Humboldt range, 9 km SW of Wells, NV. We have characterized and dated gouges from three faults exposed at Secret Pass, the main detachment fault, a subsidiary detachment above the main detachment and a high-angle normal fault in the hanging wall that soles into the low-angle detachment system. The brittle detachments are stacked vertically and are separated by <100 m in true section (Figure 2). Similar geometries of stacked low-angle detachments have been observed in the Chemehuivi Mountains of SE California and the Amargosa Chaos area of the southern Black Mountains, SE CA [*Stewart*, 1983; *Miller and John*, 1999].

4. Methods

4.1. Sampling and Clay Separation

[15] About 0.5 kg of clay gouge material was collected along a traverse across the fault core of each of the three detachment fault exposures and the hanging wall normal

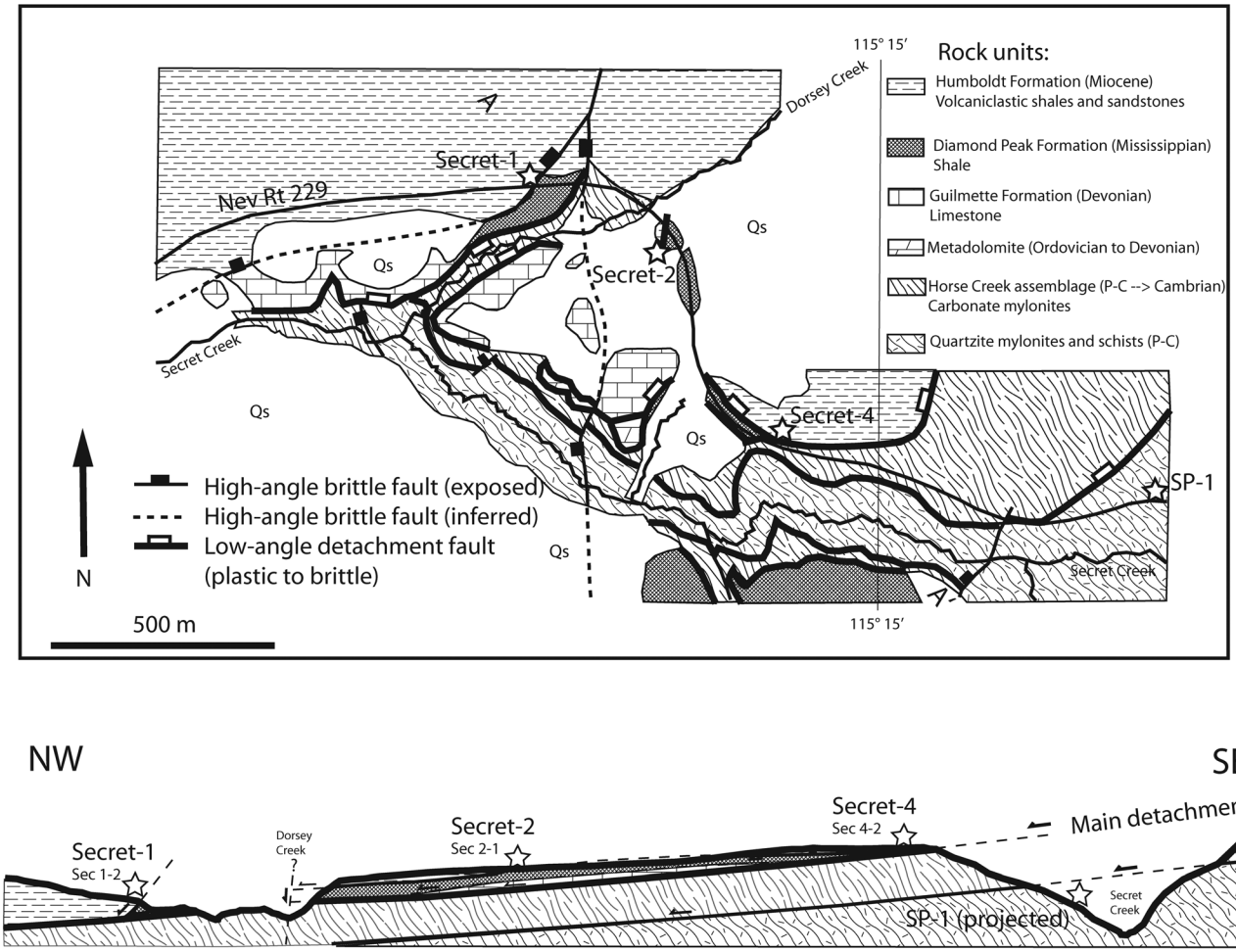

Figure 2. Simplified geologic map of the Secret Creek Gorge area and cross section showing the locations of the three detachment faults described in this paper, along with a simplified cross section along A–A′. Map redrawn from the work of *Snoke and Howard* [1984].

fault, sampling each visibly distinct region at outcrop. Samples were disaggregated by soaking in water and suspended repeatedly until the sample was free of salts. The clay-sized material (<2 μm) was separated using Stoke's law techniques. For samples of interest, the accumulated clay fraction was then centrifuged into three different size fractions (2–0.4, 0.4–0.05, and <0.05 μm) spanning roughly 2 orders of magnitude in grain size to obtain multiple samples, each with a distinct ratio of relatively coarse-grained detrital and fine-grained authigenic illitic phases. As the effects of chemical treatment to remove carbonate, quartz, or organic material on the retention of Ar by illite are not well known [*Moore and Reynolds*, 1997], we did not treat our samples further.

4.2. X-ray Diffraction

[16] To characterize the main clay minerals present in each subregion of a fault exposure, oriented clay slurry mounts of the <2 μm fraction were used. Samples were scanned from 2° to 35° 2Θ (Cu-kα) at a scan rate of 1°/min both air dried and after ethelyne glycol salvation for periods of 24 h to 7 days. The nature of illite in any illite-smectite (I/S) and the effect of any ordering (R0, R1, etc.) were determined using NEWMOD© [*Reynolds and Reynolds*, 1996]. NEWMOD calculates one-dimensional XRD patterns for (00l) reflections of illite and illite-smectite (I/S) and allows the user to vary the crystallite size, the composition of the clay phase, the percentage of illite in an illite-smectite (I in I/S) and the hydration state of that smectite, as well as any ordering in the I/S. Once the principal clay minerals were identified, illitic material was then selected for polytypism analysis. As the polytype-specific peaks used to establish the polytypism of illite are non-00*l* peaks and are suppressed by the oriented mounts used to identify the main clay minerals present, random sample preparations of the same material using a side-loaded sample packer [*Moore and Reynolds*, 1997] were used to accentuate the non-00*l* peaks. Samples were then step-scanned from 16° to 44° 2Θ with a step size of 0.05° and a count time of 40 s per step.

4.3. WILDFIRE Modeling

[17] To determine the relative abundance of the various polytypes of illite ($2M_1$ and $1M_d$) in each size fraction of illitic gouge identified by XRD scans of the oriented mounts, diffraction patterns from random XRD patterns of the same material were modeled using WILDFIRE© [*Reynolds*, 1993]. WILDFIRE© calculates three-dimensional X-ray diffraction patterns for randomly oriented grains and allows the user to change mineralogic variables to fully capture the range of structure ordering in illites described earlier, along with allowing the user to vary the thickness of the diffracting crystallites, the randomness of the sample (also known as the Dollase factor), the percentage of interlayered smectite, its hydration state and any ordering of the illite/smectite (Reichweite) [*Reynolds*, 1993]. This multitude of options allows for significantly improved matching of natural powder patterns compared with early approaches that used empirical ratios of peak areas derived from a single set of standards (see summary in the work of *Dalla Torre et al.* [1994]).

4.4. Ar-Ar Dating

[18] A total of nine clay samples from the Ruby Mountains faults were dated by the Ar-Ar method at the University of Michigan. To avoid the problem of argon recoil, the samples were packaged into fused silica vials and sealed prior to irradiation [*van der Pluijm et al.*, 2001]. Thus, the ^{39}Ar expelled from the crystallites during irradiation is retained for analysis (see *Dong et al.* [1995] for a fuller treatment of the issue). The sample vials were broken open; the initial gas was analyzed and the vials were then step-heated under a defocused laser until sample fusion occurred. The total gas age obtained from the vacuum-encapsulated sample is functionally equivalent to a conventional K-Ar age [*Dong et al.*, 1995, 1997]. Coexisting muscovite and biotite grains from footwall mylonites were also dated using standard (unencapsulated) laser step-heating techniques.

5. Results

5.1. Outcrop and Gouge Characterization

5.1.1. Secret Pass

[19] The Ruby Mountains detachment exposure in Secret Pass along Nevada Route 229 is structurally complex, with three subparallel NW dipping detachments that are exposed in roadcuts within 1 km of each other (Figures 2 and 3). The low-angle detachments are all subparallel in cross section and separate fault-bounded slices of upper-plate sedimentary rocks. The stratigraphic order of the sedimentary rocks in the fault-bounded slices is correct, i.e., younger units are found structurally above older units, but the sedimentary sequence has been radically thinned ($\gg$90%). In addition, a higher-angle normal fault in the hanging wall, which soles out onto the low-angle main detachment, is exposed [*Snoke and Howard*, 1984]. Because both the hanging wall and footwall sediments of the high-angle normal fault (Secret-1) and the upper detachment (Secret-2) show evidence for authigenic illite growth due to diagenetic processes in sedimentary basins prior to tectonic juxtaposition, detailed characterization of both the gouge and wall rocks is required.

5.1.2. High-Angle Normal Fault

[20] The high-angle fault that soles out into the main detachment is exposed in a roadcut 200 m west of Dorsey Creek (40°52′12″N, 15°15′36″W; Figures 3 and 4). The fault zone dips moderately to the northwest (52 → 320) and consists of 20–30 cm of clay-rich gouge (Figure 4). Both the footwall shale and hanging wall Miocene siltstone are highly fractured for >10 m into the wall rock. Sedimentary layering in the hanging wall within 50 m of the fault is somewhat disrupted by faulting, but relict bedding dipping 10°–20° to the north-northwest can be discerned at outcrop. Bedding in the footwall is similarly difficult to discern, owing to pervasive fracturing, but a relict gentle dip to the south-southeast at ~30° can be discerned. Neither the gouge nor the wall rock exhibit significant veining.

[21] XRD analysis of oriented and random patterns indicates that the gouge (sample Secret 1-2) consists predominantly of an illitic clay phase with a distinctive (00*l*) peak at ~11 Å (instead of the ~10 Å common to most illitic phases). Modeling the XRD patterns with NEWMOD© indicates that the phase is an illite-rich one-water I/S (75%–80% I in I/S, R0-R1) in all size fractions (Figure 4 and Table 1). The one-water layer nature of the I/S suggests that the expandable component may be a vermiculite-like mineral or a high-charge beideillite rather than smectite in a strict sense. Modeling of random powder mount XRD patterns of the same size fractions using WILDFIRE© indicates that the illite-rich I/S in Secret 1-2 is exclusively the $1M_d$ polytype (Figure 5). The hanging wall Humboldt formation (sample Secret 1-5) is a complex mixture of clay phases and contains an illite-rich illite-smectite (65%–80% I in I/S, R0-R0.5) and discrete illite (actually a second very illite-rich illite-smectite, 95% I in I/S, R0) with minor discrete smectite, chlorite, and kaolinite. The 65%–80% I in I/S dominates the finer size fractions, and is a two-water I/S (Figure 4 and Table 1). The footwall Diamond Peak shale (sample Secret 1-1) consists predominantly of discrete illite, with minor R3 I/S in the finer size fractions (Figure 4 and Table 1). Random powder mounts of Secret 1-1 indicates a clear transition from a mixture of the $2M_1$ and $1M_d$ polytypes of illite in the coarse and medium size fractions to the fine size fraction which consists exclusively of pure *tv* (transvacant) $1M_d$ illite (Figure 6). WILDFIRE modeling indicated a transition from 43% $2M_1$ in the coarse fraction to 0% $2M_1$ in the fine fraction, indicating that the fine fraction of the shale consists entirely of $1M_d$ illite, although that $1M_d$ illite is itself a mixture of discrete illite and the illite-rich R3 I/S, one or both of which might be authigenic.

[22] The authigenic, illite-rich I/S in the gouge (sample Secret 1-2) is an essentially pure one-water illite-rich I/S (80%–85% I in I/S, R0) and is thus distinct from the authigenic $1M_d$ discrete illite in the footwall (sample Secret 1-1) and the authigenic two-water illite-rich I/S (80%–85% I in I/S, R0) in the hanging wall (sample Secret 1-5), as the authigenic phases in the footwall and hanging wall are both two-water phases (Figure 4).

5.1.3. Upper Detachment

[23] A low-angle detachment above the main detachment is poorly exposed on the west side of Rt 229 near the top of a roadcut (40°52′5″N, 115°15′36″W; Figures 2 and 3) where

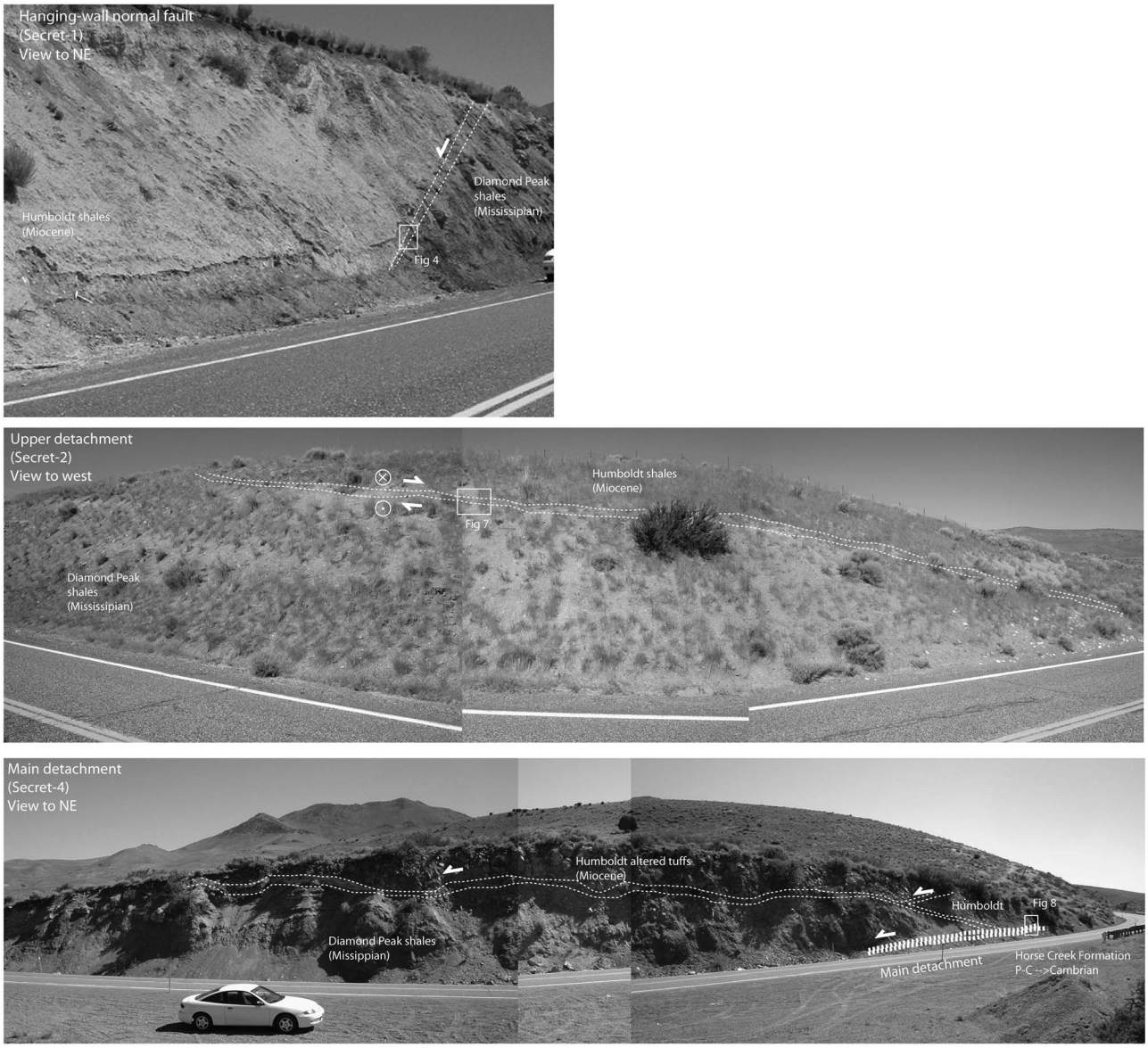

Figure 3. Field photos showing outcrops of faults at Secret Pass sampled in this study. All exposures are along NV Route 229.

it dips gently to the northwest (20 → 306). The fault zone is about 50 cm thick, clay-rich, and has relatively sharp contacts with the same footwall Diamond Peak shales and hanging wall Humboldt siltstones as the high-angle normal fault (Figure 7).

[24] The gouge zone can be divided into three distinct clay-rich regions, both visually and on the basis of XRD patterns (Figure 7). The upper region (sample Secret 2-3) consists of predominantly of illite-smectite (R1 ordered two-water layer) and kaolinite, with minor smectite. The illite/smectite is 50%–55% I in I/S, as determined by the °Δ2Θ method of *Sroden* [1980]. The central region of the gouge zone (sample Secret 2-2) is composed predominantly of R1 ordered I/S, discrete smectite, and kaolinite. Unlike the upper region, the I/S in the central region is much more illitic, 85%–90% I in I/S as determined by the °Δ2Θ method. The lower region (sample Secret 2-1) contains a complex population of illite-rich illite-smectites. Modeling with NEWMOD indicates that the coarse size fraction consists of a mixture of a 75% I in I/S R1 phase and a 55% I in I/S R0 phase. The 55% I in I/S R0 phase is more abundant in the medium and fine fractions, where NEWMOD patterns indicates that it is a one-water layer I/S, on account of its distinctive 11–12 Å basal spacing, similar to that found in Secret 1-2. The finest grain size of the gouge consists almost entirely of an illite-rich one-water layer illite-smectite (95% I in I/S, R0). A random powder XRD scan of the <0.05 μm fraction of Secret 2-1 shows that the illite-smectite consists entirely of the $1M_d$ polytype (Figure 5). The finest fraction of the gouge from the upper detachment (sample Secret 2-1)

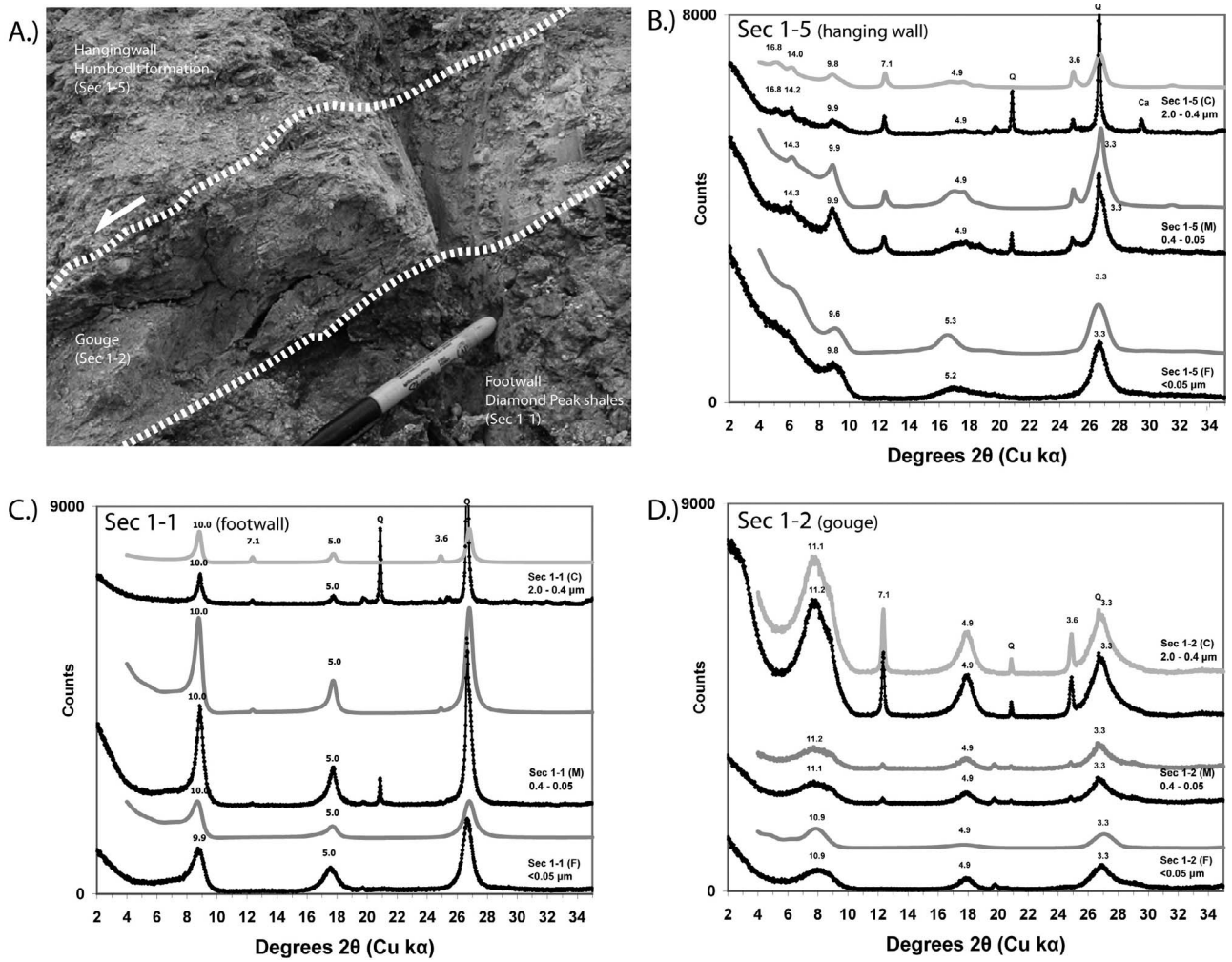

Figure 4. Field photograph and XRD patterns of <2 μm fraction from upper-plate normal fault rocks (Secret-1). (a) Field photo showing regions sampled. (b) XRD patterns (black) and matches calculated using NEWMOD$^{t©}$ (gray) for size fractions of hanging wall Miocene siltstone (Secret 1-5). (c) XRD patterns (black) and matches calculated using NEWMOD$^{©}$ (gray) for footwall Mississippian Diamond Peak shale (Secret 1-1). (d) XRD patterns of size fractions of high-angle normal fault gouge (sample Secret 1-2) and matches calculated using NEWMOD$^{t©}$ (gray). Numbers shown above phyllosilicate peaks are *d* spacings of peaks in Angstroms. All XRD patterns are oriented and glycol-solvated. Q, quartz; K, kaolinite.

is thus essentially a monomineralic $1M_d$ one-water illite-rich illite smectite (R0-R1), very similar to that of the main detachment (see below). The progression from upper to lower regions of the gouge authigenic clays of compositions 50% I in I/S, R1 → 85% I in I/S, R1 → 95% I in I/S, R0 indicates that the authigenic clay-forming reaction likely involves solid state illitization of detrital R1 I/S and the transformation of the interlayer smectite to a more vermiculite-like composition.

5.1.4. Main Detachment

[25] The main detachment fault is exposed in a roadcut along Nevada Rt 229 (40°51′53″N, 115°15′15″W; Figures 3 and 8), where the fault juxtaposes Miocene tuffs of the Humboldt Formation (heavily cemented with clinoptilite and/or heulandite) against silicified carbonate mylonites of the Horse Creek assemblage. The gouge zone is approximately 1 m thick and is mineralogically diverse. Three distinct zones can be distinguished in the gouge zone, both visually and on the basis of clay composition determined by XRD (Figure 8). The upper region of the gouge zone (sample Secret 4-1) consists of a hard light brown mixture of smectite and kaolinite, with very minor illite and quartz. The central region of the gouge zone (sample Secret 4-3) is a light green, very stiff, essentially pure smectite. The smectite is dioctahedral on the basis of a (060) reflection at 1.499 Å (61.88° Cu kα), and SEM/EDS analysis indicates that the primary cations are Mg and Fe with subordinate K and Ca, warranting the montmorillonite designation. The lower region (sample Secret 4-2) is a dark gray, hard clay consisting of illite-rich illite/smectite and quartz. The con-

Table 1. Gouge Sample Mineralogy as Determined by Analysis of Oriented XRD Patterns of Glycolated Samples Using NEWMOD

			Illitic Clays		Other Phyllosilicates			Detrital Illitic Phase			Authigenic Illitic Phase		
Structural Position	Sample	Size Fraction	% Detrital Illitic Phase	% Authigenic Illitic Phase	% Kaol	% Smec	% Chlor	% I in I/S	Ordering	Water Layers	% I in I/S	Ordering	Water Layers
High-angle normal fault - hanging wall	Secret 1-5[1]	2.0–0.4 mm	18	72	4	2	4	95	R0	2	69	R0	2
		0.4–0.05 mm	11	85	2	-	2	95	R0	2	80	R0.5	2
		<0.05 mm	-	97	-	3	-	-	-	-	66	R0.5	2
High-angle normal fault - gouge	Secret 1-2[1]	2.0–0.4 mm	45	52	3	-	-	100	-	-	77	R1	1
		0.4–0.05 mm	46	53	1	-	-	100	-	-	77	R1	1
		<0.05 mm	-	100	-	-	-	-	-	-	80	R0	1
High-angle normal fault - footwall	Secret 1-1[1]	2.0–0.4 mm	96	-	4	-	-	100	-	-	-	-	-
		0.4–0.05 mm	91	9	-	-	-	100	-	-	80	R3	2
		<0.05 mm	87	13	-	-	-	100	-	-	80	R3	2
Upper detachment - gouge	Secret 2-1[2]	2.0–0.4 mm	60	20	19	-	1	75	R1	2	55	R0	1
		0.4–0.05 mm	23	68	7	-	2	100	-	-	55	R0	1
		<0.05 mm	-	99	1	-	-	-	-	-	95	R0	1
Main detachment - gouge	Secret 4-2[3]	2.0–0.4 mm	56	37	7	-	-	85	R0	2	80	R1	1
		0.4–0.05 mm	-	95	5	-	-	-	-	-	100	R0	1
		<0.05 mm	-	100	-	-	-	-	-	-	100	R0	1
Outcrop	Latitude	Longitude											
[1]Secret-1	40° 52′ 12″	115° 15′ 36″											
[2]Secret-2	40° 52′ 6″	115° 15′ 22″											
[3]Secret-4	40° 51′ 54″	115° 15′ 17″											

tact between the upper smectite-dominated layers and the basal illitic layer is sharp but lacks any cross-cutting relationships and strongly suggests that both clay assemblages formed contemporaneously. When the basal illitic gouge (sample Secret 4-2) is separated into size fractions, a transition is evident from two distinct illite-smectite phases in the coarse size fraction to an R0 one-water layer illite-smectite within the medium and fine size fractions (Figure 8). The coarse fraction contains both a one-water 85% I in I/S with a basal spacing of 10.8 Å, and a two-water R0 80% I in I/S with a (002*) spacing of 9.8 Å. The two-water phase is absent in the 0.4–0.05 μm fraction and the <0.05 μm size fractions, indicating it is most probably detrital in origin. The R0 one-water I/S in the fine fraction in Secret 4-2 is very similar to that found as the authigenic phase in Secret 1-2 and Secret 2-1. HR-TEM observations of the clay from Secret 4-2 indicate the presence of both R1 and R3 ordering in illite-smectite together with packets of discrete illite (Figure 9). Kinks and layer terminations, indicative of lattice defects and strain, are common. X-ray texture goniometry (XTG) data (measuring clay fabric intensity) show that both the smectitic and illitic clays in the main detachment have a very weak preferred orientation [*Haines et al.*, 2009]. A random powder mount shows that the illite-smectite in Secret 4-2 consists almost exclusively of the $1M_d$ polytype in all size fractions and that the $2M_1$ polytype is either absent or present below the detection limits of XRD (typically <2%–3%; Figure 5). The finest fraction of the gouge from the main detachment (sample Secret 4-2) is thus functionally a monomineralic $1M_d$ one-water illite-rich I/S, similar to those found in the high-angle normal fault and upper detachment.

5.2. Ar-Ar Ages

5.2.1. Gouge Illite and Illite/Smectite Ages

[26] Spectra for Ar-Ar ages of the authigenic one-water, illite-rich illite-smectite isolated in the three Secret Pass samples are given in Figure 10. All the spectra have an initial near-zero age component, reflecting ^{39}Ar released during irradiation due to recoil. The percentage of Ar released during the initial "recoil" fraction ranges from 30% to 40% in all size fractions, consistent with fine-grained clays having a high surface-to-volume area and thus potential for ^{39}Ar loss during irradiation. The Ar release spectra for the main detachment and the high-angle normal fault (Secret 1-2 and Secret 4-2) do not have classic "plateaus" due to the effects of Ar recoil [*Dong et al.*, 1995], but both have a near-plateau component in the later degassing steps. The plateau-like nature of the degassing spectra are consistent with XRD observations that both samples are functionally monomineralic authigenic one-water illite-rich illite-smectite of one age population that grew apparently between 11.5 and 12.3 Ma. The sample from the upper detachment (Secret 2-1) has a "stair-step" profile more often observed in dating of authigenic illite in fault gouge [e.g., *van der Pluijm et al.*, 2001]. The stair-step geometry of the release spectra is a function of samples being composed of mixtures of grains of different ages and grain sizes. It is apparent that the Ar ages for the fine fractions of Secret 1-2 and Secret 4-2 are very close to the age of the authigenic illite-smectite growing in the fault gouge of the detachment system during fault slip, if not dating it directly. The Secret 2-1 age of 13.8 ± 0.15 Ma more likely contains some detrital material and is thus a maximum age for slip on the upper detachment.

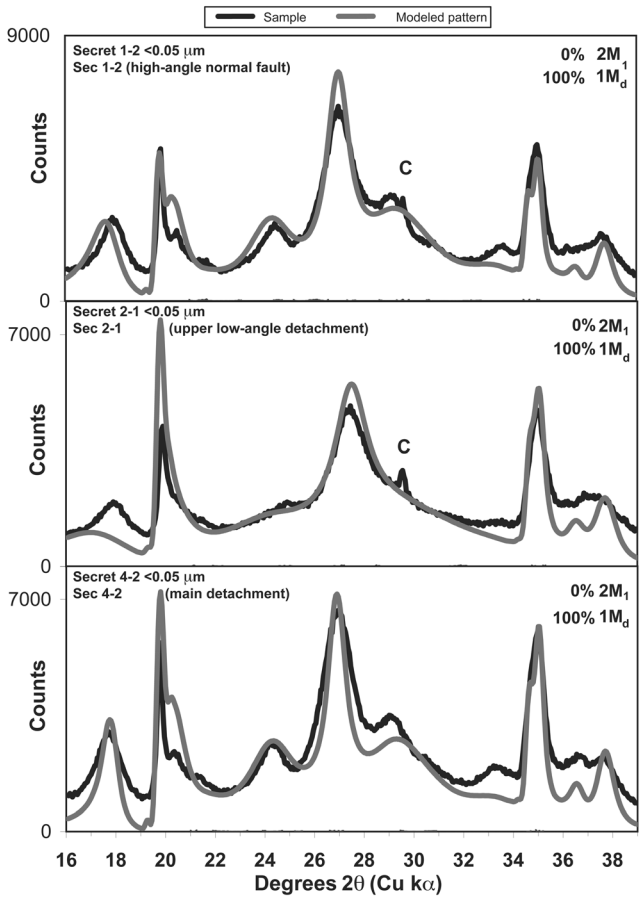

Figure 5. XRD patterns from the fine fractions (<0.05 μm) of gouges from the upper-plate high-angle normal fault (Secret 1-2), upper low-angle detachment (Secret 2-1), and main detachment (Secret 4-2), along with calculated matches using WILDFIRE©. All XRD patterns are of random powder mounts. C, calcite.

5.2.2. Footwall and Hanging Wall Illite and I/S Ages

[27] Spectra for the three size fractions of the footwall Diamond Peak shale at Secret-1 (Secret 1-1) are shown in Figure 10. All the spectra have an initial near-zero age component, reflecting ^{39}Ar released during irradiation due to recoil, with the percentage of Ar lost to recoil increasing from 20% to 30% from the coarse to fine fraction. The coarse and medium fractions have steadily climbing Ar release spectra typical of shales, while the Ar release spectrum from the fine fraction is complex. The Ar release spectrum from the fine fraction contains illites of multiple age populations, including some as old as late Paleozoic. The illite age analysis for Secret 1-1 is shown in Figure 11, indicating a poorly resolved mixture of a 532 Ma Cambrian detrital population with an authigenic 88 Ma apparently Sevier-aged population. As the Ar release spectra indicate multiple age populations of illites in the finest size fraction and the XRD modeling indicates that the finest size fraction consists exclusively of the 1Md polytype, the assumption of a two-component system cannot be made. An interpretation is offered below (see section 6). Spectra from the three size fractions of the hanging wall Humboldt formation shale (Secret 1-5) are shown in Figure 10, and an Illite Age Analysis plot is shown in Figure 11. The Ar release spectra for Secret 1-5 are all upward-climbing spectra typical of shales and indicate that all size fractions contain illites of multiple age populations. The age of the authigenic component is 10.5 ± 1.2 Ma, and the age of the detrital component is 67.0 ± 6.2 Ma.

5.2.3. Muscovite and Biotite Ages

[28] Coexisting muscovite and biotite "fish" were dated from a footwall mylonite collected 800 m east of Secret-4 and ~150 m below the detachment surface in true section (locality FW-1). Ar release spectra are shown in Figure 12. The muscovites give good plateau ages of 20.5 ± 0.1 Ma and 20.7 ± 0.1 Ma. The biotites do not have good plateaus and give conflicting ages of 12.8 ± 0.2 Ma and 15.9 ± 0.3 Ma. It is possible that the biotites were variably altered or that

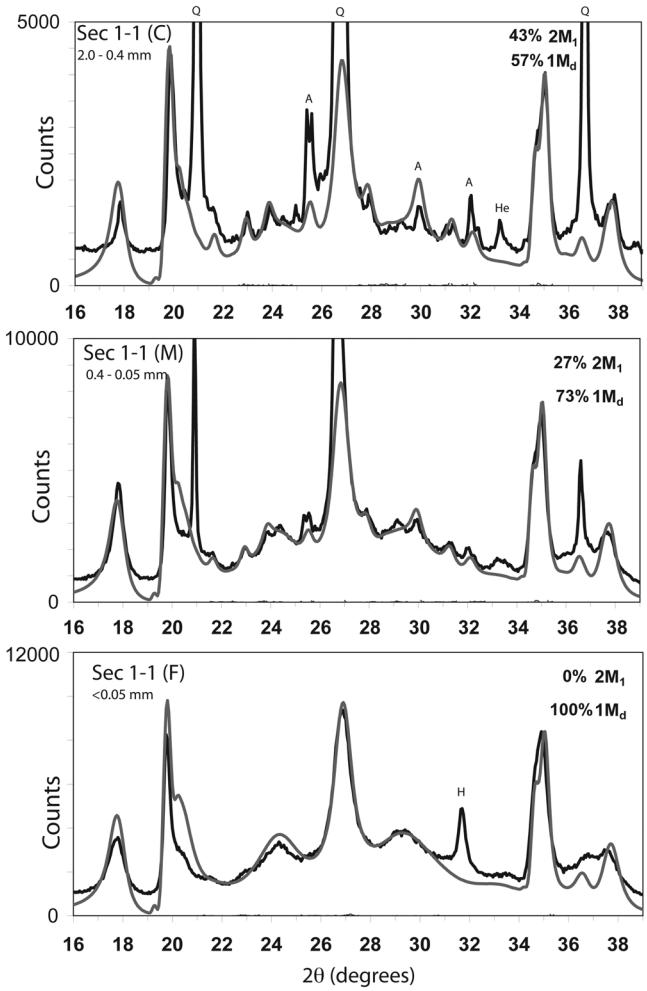

Figure 6. Illite polytypism quantifications calculated using WILDFIRE^{tm} of random-mounted size fractions of footwall of upper-plate high-angle normal fault (sample Secret 1-1) used for illite age analysis. He, hematite; H, halite; A, analcime.

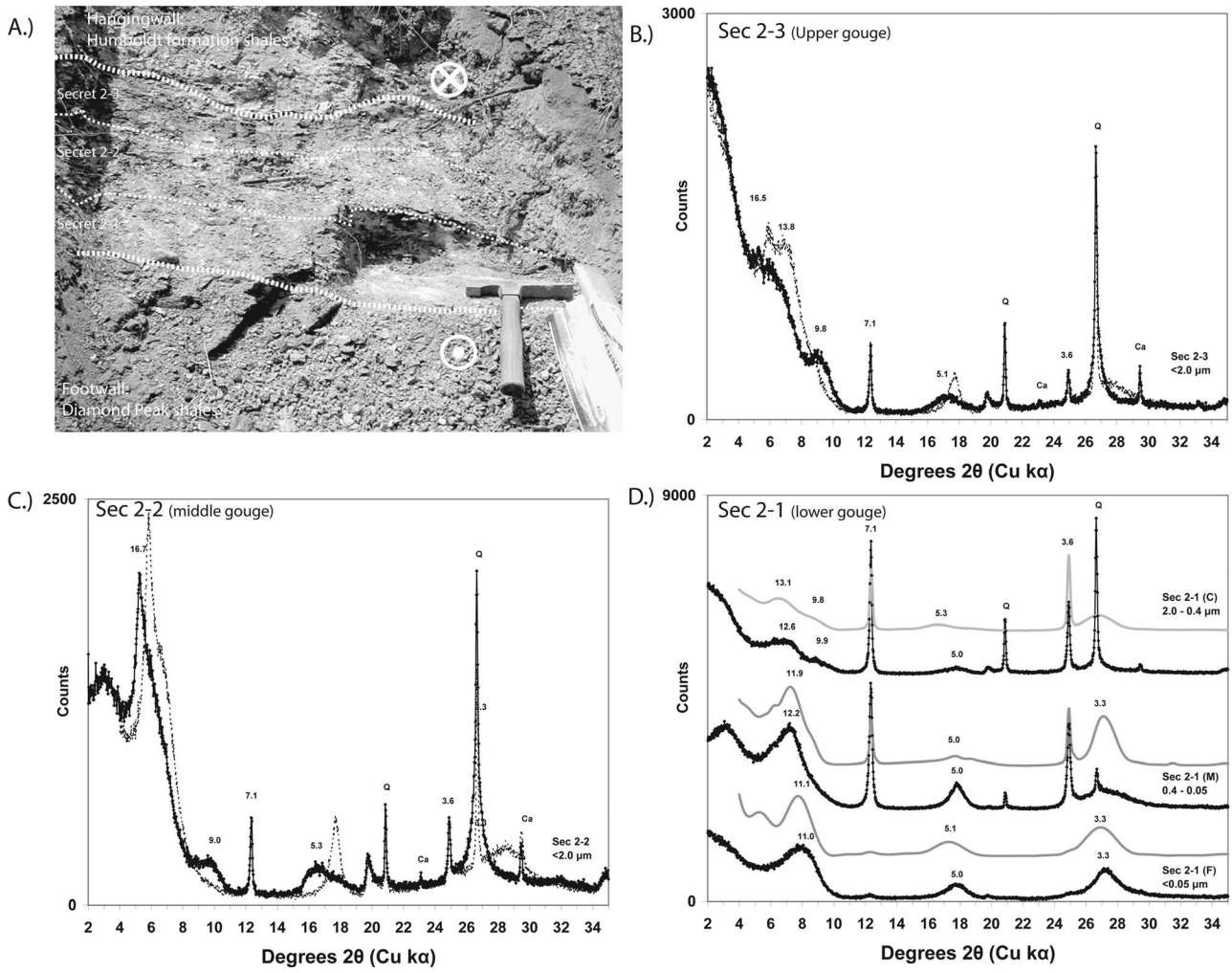

Figure 7. Outcrop photograph and XRD patterns of the <2 μm fraction of the gouge of the upper low-angle detachment (Secret 2). (a) Outcrop photo of the upper low-angle detachment, showing the three subregions sampled. (b) <2 μm size fraction of gouge from upper gouge layer (sample Secret 2-3). Dashed line is air-dried, solid line is glycol-solvated. (c) <2 μm size fraction of gouge from middle gouge layer (sample Secret 2-2). Dashed line is air-dried, solid line is glycol-solvated. (d) XRD patterns of size fractions of lower layer of upper low-angle detachment gouge (sample Secret 2-1) and matches calculated using NEWMOD© (gray). Numbers above all phyllosilicate peaks are *d* spacings in Angstroms. Q, quartz; Ca, calcite.

each grain has a different closure temperature. Petrography indicates that both quartz and feldspar deformed plastically, indicating deformation above 500°C [*Voll*, 1976; *Simpson*, 1985]. As the micas were in equilibrium with mylonitic deformation at temperatures above the blocking temperature of muscovite (375 ± 25°C) and biotite (275 ± 25°C) [*Hames and Bowring*, 1994], the Ar-Ar ages of both the muscovite (and biotite) are interpreted as cooling ages and not the age of mylonitization.

6. Interpretation and Discussion

[29] Key to the success of brittle fault dating is isolating and dating the authigenic illitic phase that grew during deformation. As both the upper detachment and hanging wall normal faults at Secret Pass juxtapose rocks that each contain one or more illitic phases, detailed clay characterization of both wall rocks and gouge is required for these rocks. The illite-rich I/S found as the authigenic phase in the clay gouges is recognizably distinct from the $1M_d$ illite or illite-rich I/S found as the authigenic phase in the wall rocks, because the authigenic phase found in the gouges is one-water I/S as opposed to the more common two-water I/S phases found in the wall rocks (see Figures 4, 7, and 8 and Table 1). Clay characterization using NEWMOD revealed the complexity of the detrital assemblages found in the wall rocks, and that two of the gouges (Secret 2-1 and Secret 4-2) contain two detrital phases, a detrital illite and a detrital illite-smectite, in addition to the authigenic one-water illite-smectite that dominates the medium and fine size fractions.

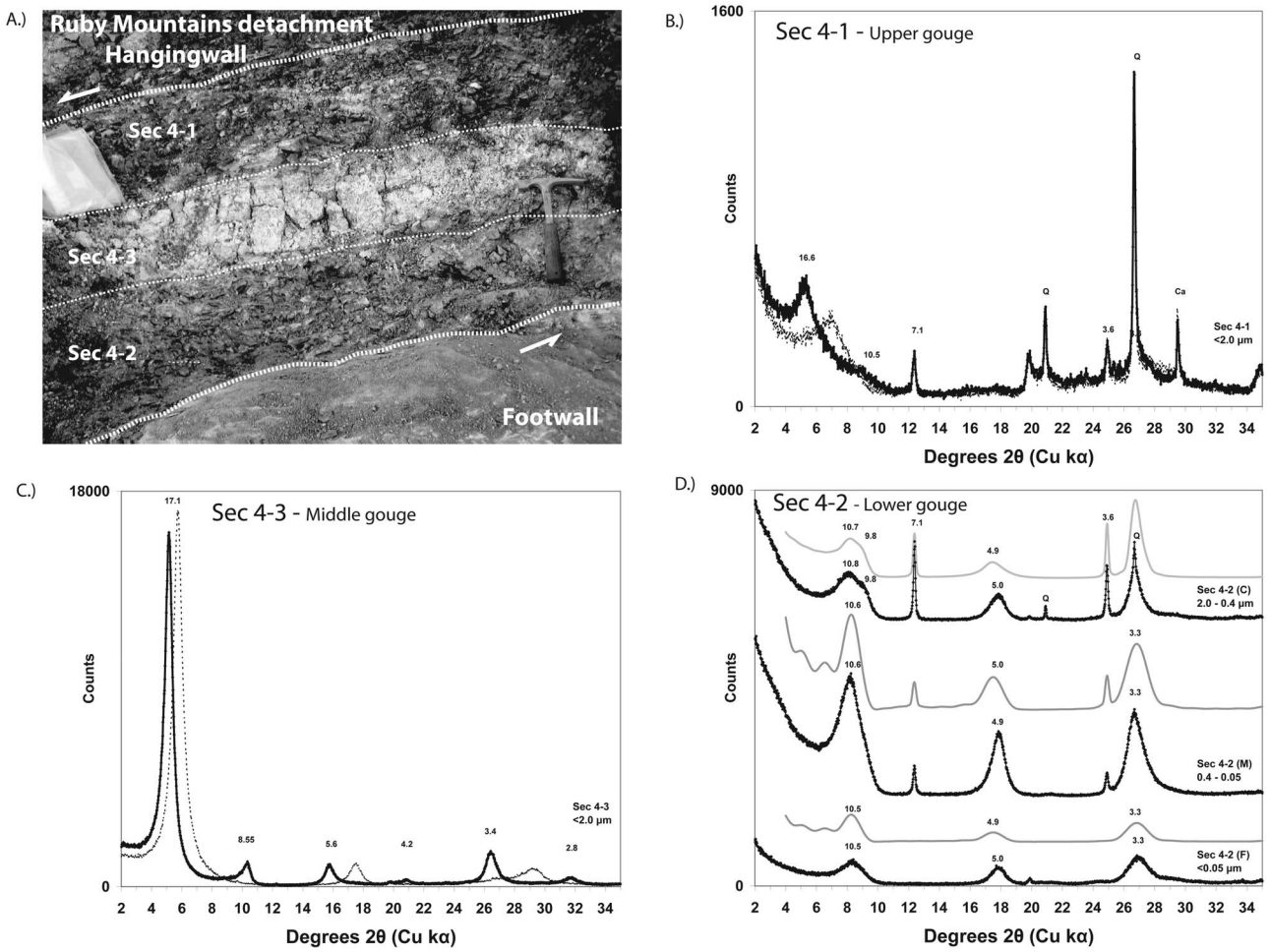

Figure 8. Outcrop photograph and XRD patterns of the <2 mm fraction of the gouge of the main low-angle normal fault (outcrop Secret-4). (a) Outcrop photo of the main detachment, showing the three subregions sampled. (b) <2 μm size fraction of gouge from upper gouge layer (sample Secret 4-1). Dashed line is air-dried, solid line is glycol-solvated. (c) <2 μm size fraction of gouge from middle gouge layer (sample Secret 4-3). Dashed line is air-dried, solid line is glycol-solvated. (d) XRD patterns (black) and matches calculated using NEWMOD$^{t©}$ (gray) for size fractions of gouge from lower gouge layer (sample Secret 4-2). Numbers above all phyllosilicate peaks are *d* spacing in Angstroms. Q, quartz; Ca, calcite.

Illite age analysis (which uses a binary mixture of one detrital phase and one authigenic phase) is therefore inappropriate for these gouges, as the assumption of a binary mixture between one detrital and one authigenic phase cannot be guaranteed. Extracting a meaningful age from complex mixtures (>2 illitic components) requires that the authigenic phase concentrated in the finest size fraction (<0.05 μm) be characterized to demonstrate the material is both monomineralic and contains only one polytype using both NEWMOD© and WILDFIRE. The relative uniformity of the Ar-Ar spectra degassing is then used to further check whether the material is of one age population. For the upper-plate high-angle normal fault and main detachment (Secret 1-2 and Secret 4-2), this argument can be successfully made and we obtain ages that date the formation of the gouges. The spectra for Secret 2-1 is strongly sloped and indicates that it contains more than one age population of illite-rich illite-smectites that are otherwise indistinguishable by XRD methods. The 13.8 Ma age from Secret 2-1 is thus a maximum age for gouge formation.

[30] The ages of the footwall Diamond Peak shale and hanging wall Humboldt Formation are complex but are interpretable in light of tectonic activity on the detachment system at 11–13 Ma. Previous dating studies of fault gouges have recorded the age of gouge formation in wall rocks within 50 m of the fault zone [*Vrolijk and van der Pluijm*, 1999; *Solum and van der Pluijm*, 2007], and it is probable that both the hanging wall and footwall ages reflect some illite growth during active faulting in addition to earlier ages inherited during sediment deposition and subsequent diagenesis. For the footwall Diamond Peak formation, the age of the authigenic component extrapolated from illite age analysis of 86 Ma is interpreted as a Sevier age of growth of $1M_d$ illite, as the polytypism analysis using WILDFIRE

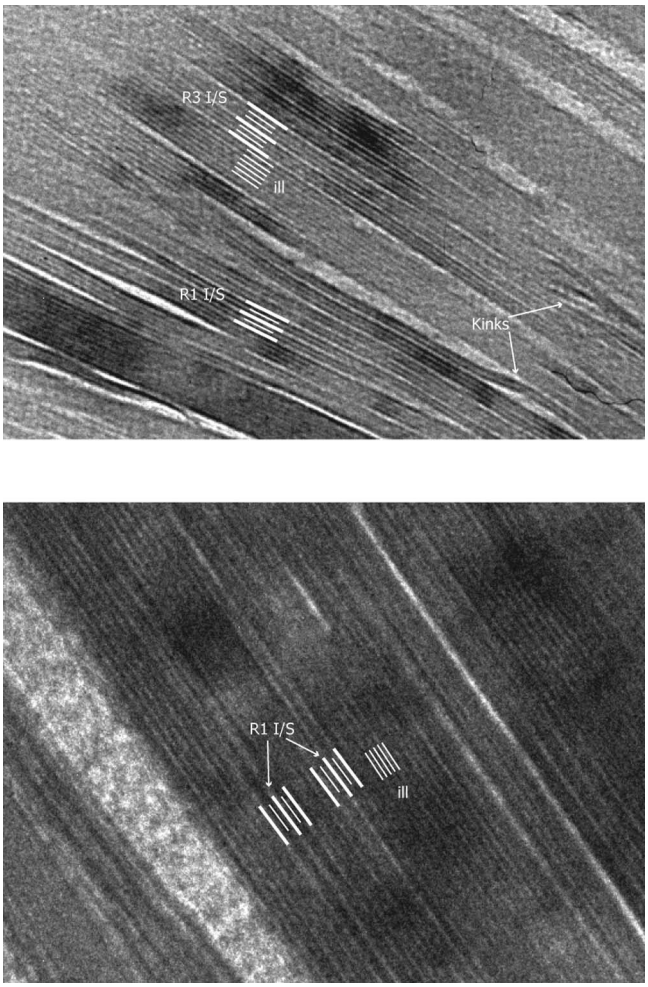

Figure 9. HD-TEM lattice fringe images of clays from the main detachment (Secret 4-2). Thin (5–10 nm) packets of ordered illite-smectite (both R1 and R3) are visible together with 8–20 nm packets of illite. Kinked layers, indicative of strain, are visible in the upper image.

indicates a clear transformation between coarse and medium size fractions that contain significant amounts of the $2M_1$ polytype (typically detrital muscovite) component and a fine fraction that consists entirely of the authigenic $1M_d$ polytype that typically grows during burial diagenesis. However, the NEWMOD modeling of the same fine fraction (<0.05 μm) indicates that the fine fraction contains both discrete illite and illite-rich I/S. The degassing spectra for Secret 1-1 (F) also record the presence of some 250–350 Ma material in the <0.05 μm size fraction, even though WILDFIRE modeling indicated the material consisted entirely of the $1M_d$ polytype. A possible interpretation of the 86 Ma extrapolated age for the authigenic component of the footwall shales is a Pennsylvanian-Permian $1M_d$ component inherited from initial burial diagenesis and a much younger second episode of authigenic $1M_d$ illite growth either during Sevier times or during faulting. The 525 Ma age extrapolated for the detrital component may reflect sediments of the Diamond Peak that were sourced from an area with late Precambrian cooling ages.

[31] The depositional age of the Humboldt Formation is Miocene and must be greater than 15.0 Ma, based on field relationships. The 10.6 Ma age of the authigenic two-water illite-smectite in the hanging wall as extrapolated from illite age analysis is close to the 11.6 Ma age of the authigenic one-water illite-smectite in the gouge, although the age of authigenic I/S growth in the hanging wall is slightly younger. It is possible that the same fluids that were responsible for the growth of I/S in the gouge continued to circulate in the highly fractured hanging wall after the main pulse of tectonism and gouge formation ceased.

[32] The illite-rich nature of authigenic I/S constrains the conditions of authigenic clay growth in the gouge. The smectite-illite transition has been extensively studied in sedimentary basins [e.g., *Hower et al.*, 1976; *Ahn and Peacor*, 1986; *Freed and Peacor*, 1989a, 1989b; *Li et al.*, 1997; *Kim et al.*, 2004; *Huggett and Cuadros*, 2005; *Sandler and Saar*, 2007]. While the transformation is generally agreed to be a prograde diagenetic series of reactions below 200°C, numerous factors besides temperature can control the progress of the reactions. Time [*Pytte and Reynolds*, 1989], K+ availability [*Huang et al.*, 1993], water/rock ratio [*Whitney*, 1990], and microbial interactions [*Kim et al.*, 2004] have all been shown to affect reaction progress. As discrete nonillitic smectite can form in soils and has been shown to be stable to temperatures as high as ~135°C in sedimentary basins [*Aplin et al.*, 2006] and authigenic ordered I/S forms in evaporative environments at temperatures of <45°C [*Sandler and Saar*, 2007], constraints on the temperature of I/S growth are thus poor, except that clay growth occurred <200°C and probably between 50°C and 150°C. While illite-rich illite-smectite is know from active and fossil hydrothermal systems at temperatures up to 285°C [e.g., *Junfeng et al.*, 1997], the absence at outcrop for evidence of the pervasive hydrothermal alteration associated with hydrothermal systems (quartz and calcite veining, adularia, etc.) indicates that the larger temperature range observed for the stability of illite-smectite in open hydrothermal systems is not appropriate for detachment faults. Field relations of the illite-rich layer and the smectite-rich layers in the main detachment are consistent with both phases forming at the same time, which therefore constrains the temperature to ~50°C–135°C. The smectite-rich upper

Figure 10. ^{40}Ar-^{39}Ar illite step-heating spectra for vacuum-encapsulated clay gouge size fractions dated at Secret Pass. Left-hand column is spectra from three size fractions of footwall of high-angle normal fault (sample Secret 1-1). Center column is spectra from three size fractions of hanging wall of upper low-angle normal fault (sample Secret 1-5). Right column is spectra from the fine fractions (<0.05 mm) from the three one-water I/S gouges Secret 1-2, Secret 2-1, and Secret 4-2 (<0.05 mm fractions from the high-angle normal fault, upper low-angle detachment, and main low-angle detachment, respectively).

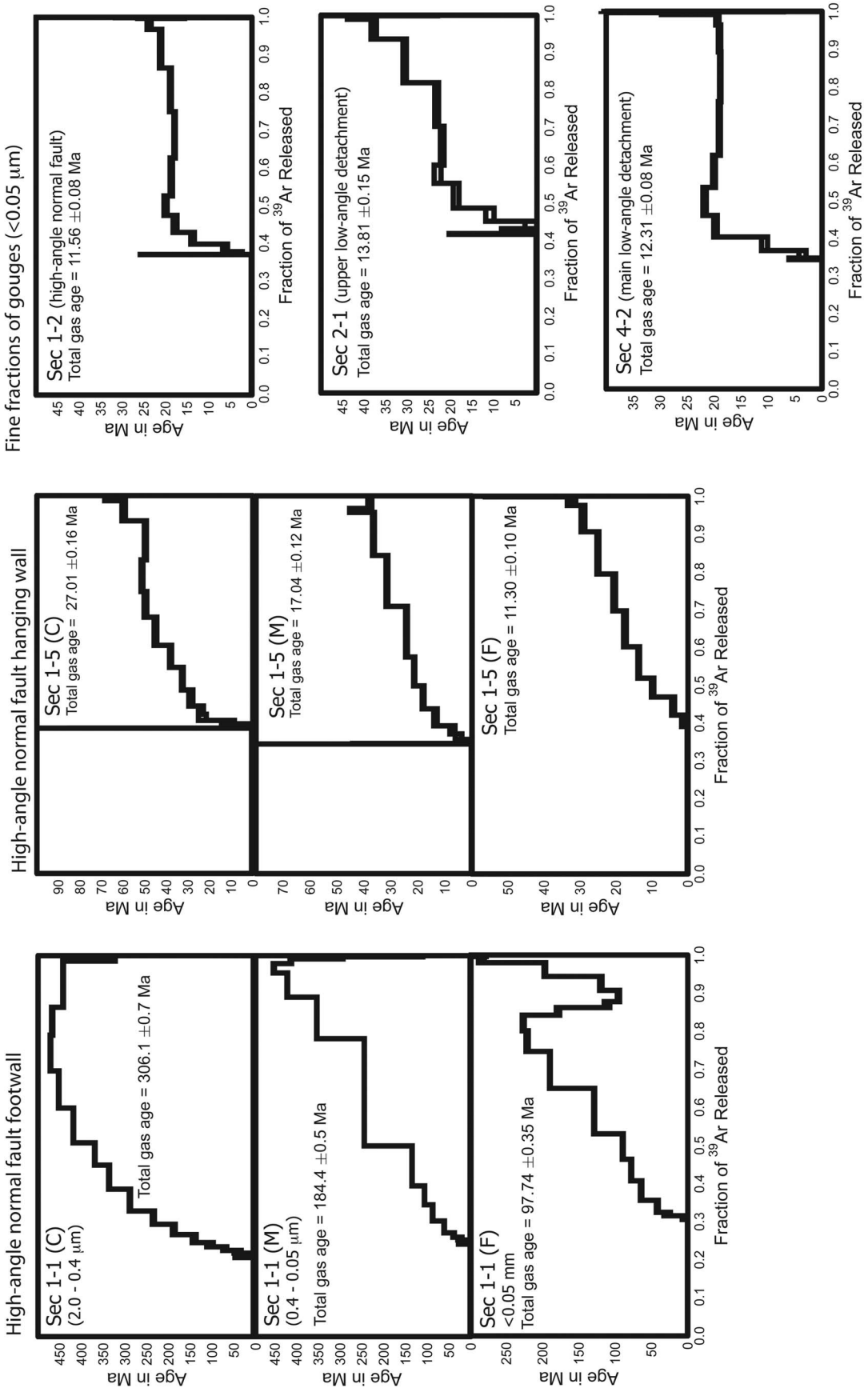
High-angle normal fault footwall
Sec 1-1 (C)
(2.0 - 0.4 μm)
Total gas age = 306.1 ±0.7 Ma
Sec 1-1 (M)
(0.4 - 0.05 μm)
Total gas age = 184.4 ±0.5 Ma
Sec 1-1 (F)
<0.05 mm
Total gas age = 97.74 ±0.35 Ma
High-angle normal fault hanging wall
Sec 1-5 (C)
Total gas age = 27.01 ±0.16 Ma
Sec 1-5 (M)
Total gas age = 17.04 ±0.12 Ma
Sec 1-5 (F)
Total gas age = 11.30 ±0.10 Ma
Fine fractions of gouges (<0.05 μm)
Sec 1-2 (high-angle normal fault)
Total gas age = 11.56 ±0.08 Ma
Sec 2-1 (upper low-angle detachment)
Total gas age = 13.81 ±0.15 Ma
Sec 4-2 (main low-angle detachment)
Total gas age = 12.31 ±0.08 Ma
Age in Ma
Fraction of ^{39}Ar Released

Figure 10

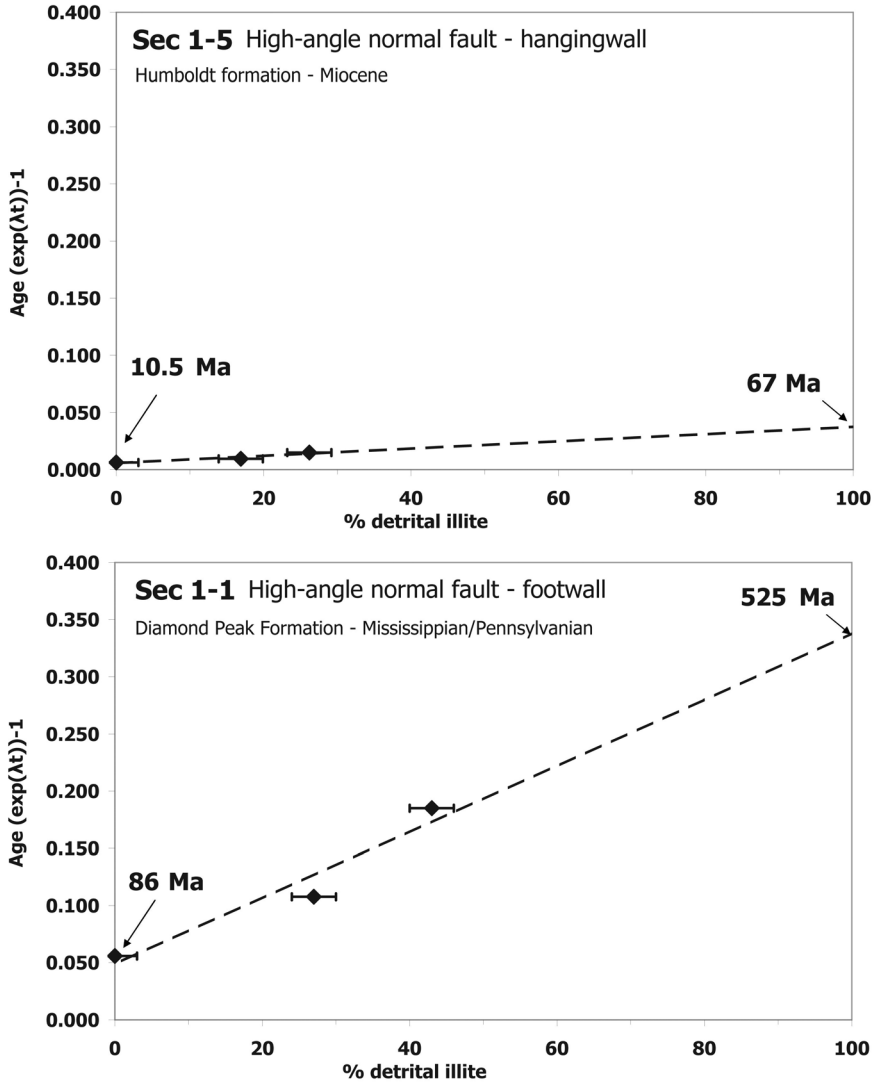

Figure 11. Illite age analysis plots for the hanging wall and footwall rocks of the upper-plate high-angle normal fault. (top) IAA plot for sample Secret 1-5 (Humbold Formation, Miocene, >15.0 ± 1.5 Ma depositional age) [*Snoke and Howard*, 1984]. (bottom) IAA plot for sample Secret 1-1 (Diamond Peak shale, Mississippian) [*Snoke and Howard*, 1984].

and central layers at the main detachment derived from alteration of the hanging wall silicified tuffs, while the basal I/S-rich layer is derived from retrograde alteration of smeared Diamond Peak shale. At Secret-4, the footwall at the sampled outcrop is a carbonate mylonite, and not Diamond Peak shale, but the outcrop is only 20 m updip from outcrops of Diamond Peak in the hanging wall (Figure 3), and thus Diamond Peak shale was most probably smeared along the fault surface at the sampled location. The components of the authigenic, one-water illite-smectite, also found within the upper detachment and high-angle normal fault, could be derived from either the further illitization of I/S derived from the hanging wall shales or by dissolution and reprecipitation of illite derived from the footwall Diamond Peak shales. The presence of both detrital I/S and detrital discrete illite populations in the coarse fraction (2.0–0.4 μm) of the gouges suggests some combination of sources is likely.

[33] The ^{40}Ar-^{39}Ar ages of illite in the finest size fractions from the gouges at Secret Pass, which date the age of fault gouge formation, show that the last major period of activity on the main detachment fault occurred at ~12.3 Ma and that the last major period of activity on the hanging wall high-angle normal fault occurred at ~11.5 Ma. The upper detachment was last active at some point after 13.8 Ma. The closure temperature of illite is somewhat grain-size dependent but is >250°C for very fine-grained illite and muscovite [*Hall et al.*, 2000]. Our illite ages are thus growth ages and not cooling ages, as the temperatures at which the authigenic clay grew (50°C–135°C) are far below the closure temperature of Ar diffusion. Importantly, the similar ages and mineralogies of the authigenic components indicate that the two low-angle

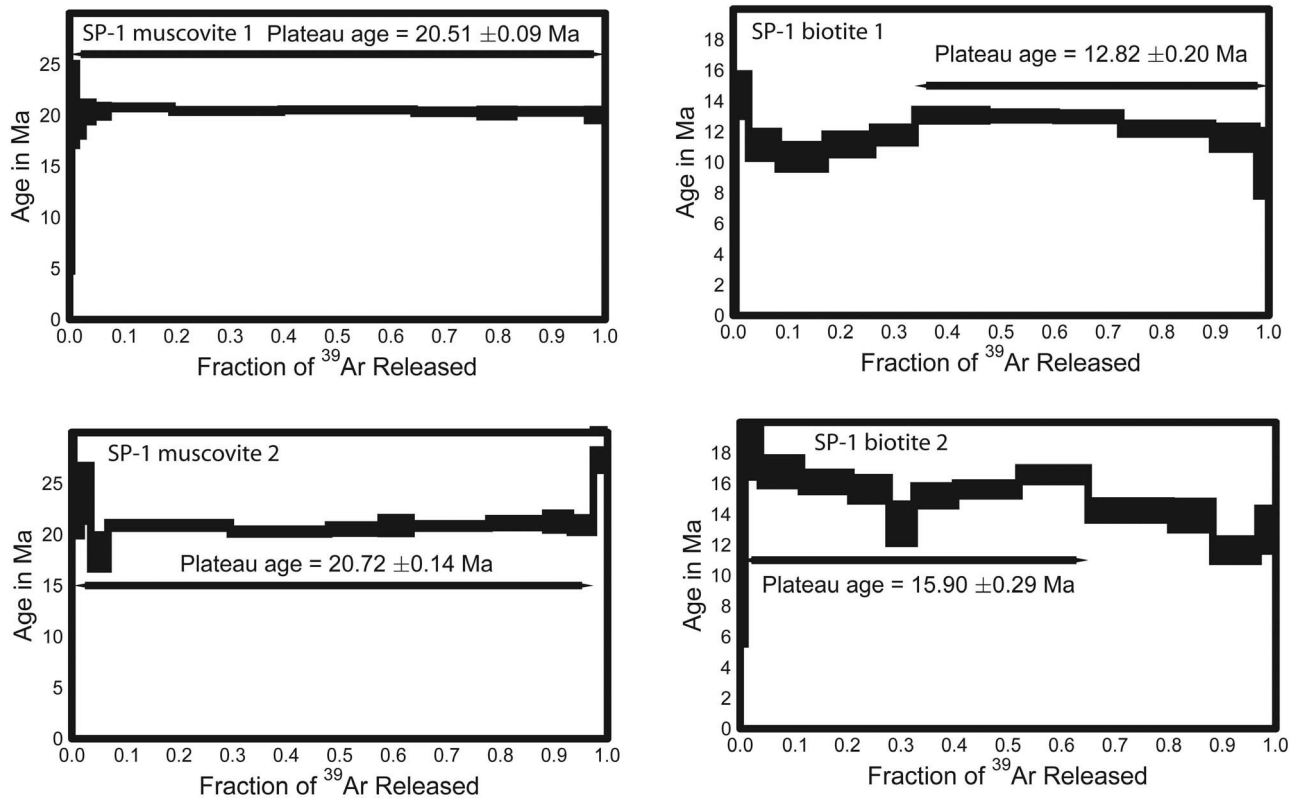

Figure 12. ^{40}Ar-^{39}Ar illite step-heating spectra for coexisting muscovite and biotite from quartzite mylonites at Secret Pass (locality SP-1).

faults and the high-angle normal fault were all active at the same time as part of a kinematically linked fault system.

[34] The preferred explanation for our illite ages is that both the high-angle upper-plate normal fault and both low-angle detachments were all active at the same time at about 11–13 Ma. We believe that the Ar-Ar age of a single size fraction of the pure authigenic component of a clay gouge is a sample of a suite of ages that span the time period over which the authigenic illitic gouge grew and thus that the analytical error estimates from a single age measurement are smaller than the age range of the suite of authigenic illites measured. However, the presence of a minor but significant detrital component as indicated by the Ar-Ar spectra of the authigenic component of Secret 2-1 (the upper low-angle detachment) and the resulting age being only 1.5 Ma older than illitic gouge from the main detachment and 2.3 Ma older than the age of the authigenic component of gouge from the high-angle normal fault strongly suggest that all three gouges formed roughly coevally. The coincidence of coeval gouge formation in all three faults is further supported by the similarity of the distinctive one-water layer illite-rich smectites found as the authigenic component of the gouges in all three faults.

[35] Contemporaneous formation of clay gouges of normal faults with contrasting orientations has implications for the kinematics of metamorphic core complex detachments. The similarity of ages of the gouges from all three faults indicates that normal faults with varying orientations were active coevally and places constraints on the dip of both the low-angle detachment faults and the high-angle normal fault at the time of slip. The current dip of the high angle fault (52°) is at the low end of the typical dips observed for high-angle normal faulting (45°–70°) [*Jackson and White*, 1989], although higher-angle normal faults with a clear kinematic link to detachment faults (based on clear field relations) have been observed to have a wide range of dips ranging from 45° to >80° [e.g., *Anderson*, 1971; *Hayman et al.*, 2003]. The Miocene sediments in the hanging wall of the high-angle normal fault dip shallowly to the north (obliquely down-dip) and do not "roll over" into the high-angle normal fault. The absence of significant rollover and the overall low dip of the hanging wall sediments in the high-angle normal fault suggest that significant rotation of the hanging wall of the high-angle normal fault has not occurred. Assuming a maximum 38° rotation of the footwall to account for a 52°–90° range in possible initial dips of the high-angle normal fault, the dip of the low-angle detachments would rise to no more than 48° at the time of fault slip (Figure 13). We thus conclude that the degree of postslip rotation of the normal faults in the Secret Pass area is <~30°, although rotation of up to 38° is possible. We also conclude that the low-angle detachments in the Secret Pass area were active in the brittle regime at dips <~30° at 11–13 Ma, which is inconsistent with the passage of a "rolling hinge" in a strict sense in the uppermost crust, assuming a maximum footwall rotation (>40°) in the Secret Pass area. Rather, the

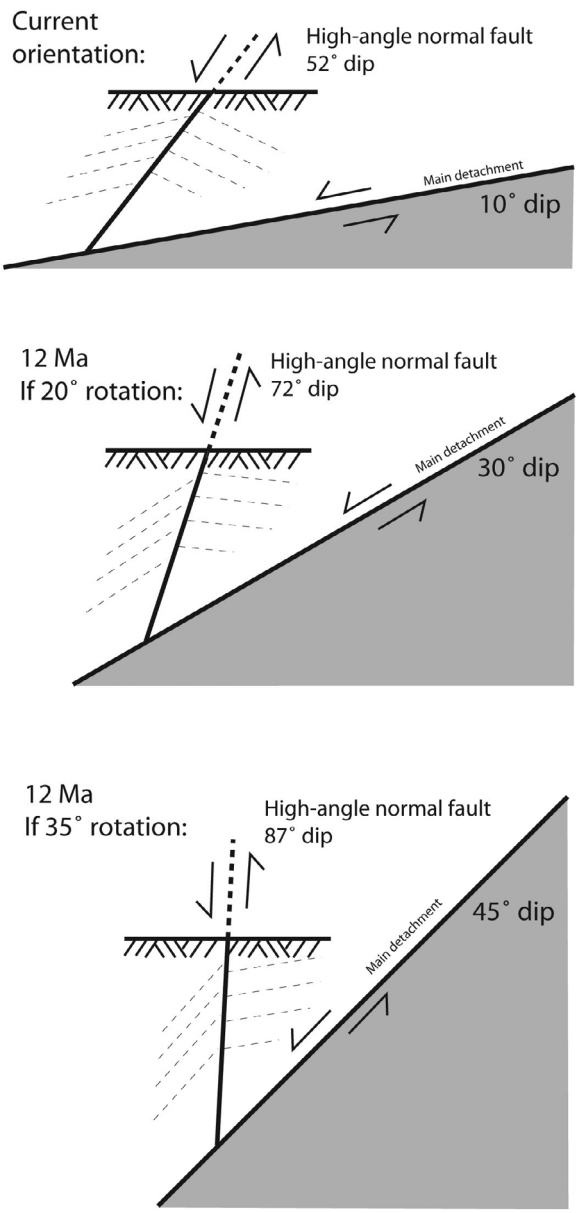

Figure 13. Sketch showing constraints on the amount of postfaulting footwall rotation on dips of Secret Pass faults active at 11–13 Ma, and thus, the dips at which the detachment fault system was active. The Ar-Ar ages of the gouge demonstrate that both the low- and high-angle faults were active at roughly the same time from 11 to 13 Ma. A rotation of 20° permits slip on the main detachment allows the upper-plate normal fault to initiate at 70°, a typical angle for a high-angle normal fault, and obeys rock mechanics constraints for coefficient of friction (μ) = 0.4; 35° of postfaulting rotation also satisfies rock mechanics but requires that the high-angle normal fault initiate as a near-vertical fracture. Dashed lines are traces of the bedding of the footwall and hanging wall blocks of the high-angle normal fault projected on a WNW-ESE section.

fault ages are consistent with either (1) detachment slip at dips <45° and potentially at dips of >22°, while still obeying principles of fault mechanics (see below) or (2) detachment slip at or near the current low dip of 10°, with our preferred explanation being the first. Our data suggest that the Ruby Mountains detachment was accommodating extension on a primary low-angle normal fault surface as envisaged by *Spencer* [1984], with some postfaulting footwall rotation (<20°) instead of large-magnitude flexural rotation (>45°) of the footwall, as envisaged by the models of *Wernicke and Axen* [1988], *Buck* [1988], or *Hamilton* [1988]. It is important to note that our ages do not constrain either the dip of the detachment at its initiation in the Middle Eocene or the kinematics of earlier slip at deeper crustal levels, but rather the kinematics of the final stages of detachment evolution during the Middle Miocene.

[36] The frictional properties of clay gouges from low-angle normal faults are an area of considerable uncertainty, but experimental friction results [*Saffer and Marone*, 2003; *Tembe et al.*, 2006, 2009; *Numelin et al.*, 2007] indicate that illite-rich sediments and illite-rich dry gouges have a coefficient of friction of ~0.4–0.5 at stress conditions similar to those reasonable for gouge formation; i.e., significantly lower than the 0.65–0.8 indicated by Byerlee friction. Such results place further constraints on the angle of slip of the detachment fault at the time of gouge formation. Slip at dips of >22° is thus possible with a coefficient of friction of 0.40 without violating Mohr-Coulomb criteria for slip at hydrostatic stress conditions, as the tangent of 22° is 0.40. Both the kinematic constraints imposed by the similarity of the ages of clay gouge from all three faults in the detachment system, and the likely frictional strength of the gouges indicate that the detachment could have slipped at dips only 12° higher than the current dip of 10°. While some postfaulting rotation undoubtedly occurred, its magnitude cannot be more than 38° (imposed by the dip of the hanging wall normal fault) and could be as low as ~12° without violating conventional fault mechanics. A large-magnitude rotation of the footwall, as might be expected from the passage of an upper-crustal "rolling hinge" is thus, strictly speaking, impossible, while a smaller rotation due to gradual extension, with rotation to dips lower than are commonly observed in "typical" normal faults aided by the growth of lower-friction authigenic illite-smectite in the fault zone, seems likely. Similar gradual rotation of the detachment to low dips with increasing fault slip has been shown at other core complexes [*Wong and Gans*, 2008].

[37] The higher-temperature muscovite and biotite Ar-Ar ages provide constraints on the rate of exhumation of older portions of the detachment system. The mylonites at Secret Pass clearly formed earlier than 20 Ma, as they record amphibolite facies conditions during mylonitization, significantly higher than the Ar-Ar closure temperature of muscovite. Figure 14 shows the time-temperature history of the footwall from the Secret Pass area from this study and previously published data. The coexisting muscovite and biotite ages, together with the gouge ages at Secret Pass, define a consistent time-temperature path extending from the onset of exhumation in the latest Eocene and extending into the middle-late Miocene, with an increase in cooling

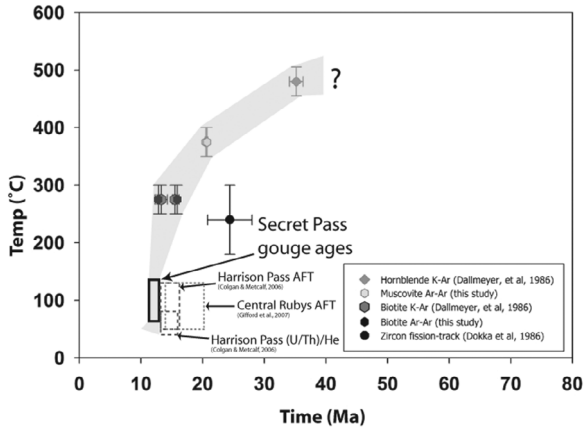

Figure 14. Exhumation history for Secret Pass as inferred from data from this study and published sources. Gouge ages and muscovite ages are from this study. Biotite ages are from this study and *Dallmeyer et al.* [1986]. Hornblende Ar-Ar ages are from the work of *Dallmeyer et al.* [1986], Zircon fission track age is from the work of *Dokka et al.* [1986]. Central Ruby Mountains and Harrison Pass apatite fission track and apatite (U/Th)/He ages from the works of *Colgan and Metcalf* [2006] and *Gifford et al.* [2007] are plotted as dashed lines for reference, although they are located 30 and 65 km, respectively, to the southwest along strike from Secret Pass.

rate between biotite closure at 13–15 Ma and gouge formation at ~12 Ma. However, the zircon fission track age of *Dokka et al.* [1986] from the same locality does not fall on the time-temperature path defined by our Ar ages and more recently reported thermochronometer ages from farther south in the range along strike. *Colgan and Metcalf* [2006] report 14–15 Ma apatite fission track ages and apatite (U/Th)/He ages from the Harrison Pass area, approximately 65 km to the southwest along strike. *Gifford et al.* [2007] report 20.4–14.1 Ma apatite fission track ages from the central Ruby Mountains, approximately 30 km to the southwest along strike, with ages younging to the west-northwest (down-dip). Instead of middle- to late-Miocene exhumation documented by several isotopic systems, the zircon fission track age implies very rapid exhumation during the late Oligocene. We submit that the *Dokka et al.* [1986] zircon fission track age is not geologically meaningful and perhaps erroneous. The gouge ages also indicate that exhumation of the core complex through the ~100°C isotherm may have progressed from south to north from ~15 Ma at Harrison Pass to ~12 Ma at Secret Pass and that gouge formation at Secret Pass may represent the very end of activity on the Ruby Mountains detachment. Assuming a geothermal gradient of 25°C/km, a fault dip of 30° and growth conditions for illite-rich I/S of ~100°C, the detachment fault accommodated 22 km of slip between 20.5 and 12.0 Ma, implying a net slip rate of 2.6 ± 0.7 mm/yr and a strain rate on the order of 10^{-14} s^{-1}, with a likely acceleration between 14 and 12 Ma. As the coeval ages of the brittle faults prohibit a dip >38° for the main detachment at the time of gouge growth, the dip of the detachment could be as low as current values (~10°), although recent results from rock friction experiments suggest that dips >22° are more likely. Similar mean slip velocities on the order of millimeter per year have been reported from other core complex detachment faults [*Carter et al.*, 2006; *Haines and van der Pluijm*, 2008].

7. Conclusions

[38] Our XRD and Ar-Ar study indicates that authigenic one-water layer illite-rich I/S grew in fault gouge from the Secret Pass area of the Ruby Mountains, Nevada at 11–13 Ma. The authigenic illite-rich I/S in gouge is distinguishable from illite and illite-smectite derived from the wall rocks on the basis of mineralogy and hydration state, as determined by XRD and TEM analyses. An interpretation that illite-smectites and $1M_d$ illite in both the gouge and the wall rock are the products of a common postfaulting diagenetic event is unlikely, as the rocks do not show any evidence for a postfaulting hydrothermal event, and the area has been exhumed post12 Ma, instead of buried. Ar ages of the authigenic illite in two detachment faults and a high-angle fault that soles into the detachment system show that the high-angle normal fault and the main detachment fault formed around 11–13 Ma and that gouge in the upper low-angle detachment formed <13.8 Ma. Exhumation of the Ruby Mountain metamorphic core complex in the vicinity of Secret Pass thus occurred during the middle-late Miocene, with fault slip averaging 2.6 ± 0.25 mm/yr and the last major period of slip around 12 Ma. The gouge ages indicate that all three faults were active at the same time and thus part of a kinematically linked system in the frictional regime, with the main detachment surface at dips <45° and potentially as low as 22°.

[39] **Acknowledgments.** This work was supported by NSF grant EAR 0738435, exploratory funding by a GSA grant-in-aid to Haines, and the Scott Turner Fund at the University of Michigan. We are grateful to Chris Hall and Marcus Johnson for assistance with Ar dating, to Carl Henderson for maintenance of the EMAL X-ray facility at Michigan, and to Anja Schleicher for assistance with microscopic characterization. Nick Hayman and an anonymous reviewer provided thoughtful reviews that significantly improved the presentation of this study.

References

Abers, G., C. Mutter, and J.-F. Fang (1997), Shallow dips of normal faults during rapid extension: Earthquakes in the Woodlark-D'Entrecasteaux rift system, Papua New Guinea, *J. Geophys. Res.*, *102*, 15,301–15,317, doi:10.1029/97JB00787.

Ahn, J., and D. Peacor (1986), Transmission and analytical electron microscopy of the smectite-to-illite transition, *Clay. Clay Miner.*, *34*, 165–179.

Anderson, E. (1942), *The Mechanics of Faulting and Dyke Formation With Respect to Britain*, 191 pp., Oliver and Boyd, Edinburgh.

Anderson, R. E. (1971), Thin-skin distension in Tertiary rocks of southwestern Nevada, *Geol. Soc. Am. Bull.*, *82*, 43–58.

Aplin, A., I. Matenaar, D. McCarty, and B. van der Pluijm (2006), Influence of mechanical compaction and clay mineral diagenesis on the microfabric and pore-scale properties of deep-water Gulf of Mexico mudstones, *Clay. Clay Miner.*, *54*, 500–514.

Axen, G. (2004), Mechanics of low-angle normal faults, in *Rheology and Deformation of the Lithosphere at Continental Margins*, edited by G. Karner et al., pp. 45–91, Columbia.

Byerlee, J. (1978), Friction of rocks, *Pure Appl. Geophys.*, *16*, 615–626.

Buck, W. (1988), Flexural rotation of normal faults, *Tectonics*, *7*, 959–973, doi:10.1029/TC007i005p00959.

Carter, T., B. Kohn, D. Foster, A. Gleadow, and J. Woodhead (2006), Late stage evolution of the Chemehuevi and Sacramento detachment faults from apatite (U/Th)/He thermochronometry–Evidence for mid-Miocene accelerated slip, *Geol. Soc. Am. Bull.*, *118*, 689–709.

Chiaraluce, L., C. Chiarabba, C. Collettini, D. Piccinini, and M. Cocco (2007), Architecture and mechanics of an active low-angle normal fault: Alto Tiberina fault, northern Appenines, Italy, *J. Geophys. Res.*, *112*, B10310, doi:10.1029/2007JB005015.

Cichanski, M. (2000), Low-angle range-flank faults in the Panamint, Inyo and Slate ranges, California: Implications for recent tectonics of the Death Valley region, *Geol. Soc. Am. Bull.*, *112*, 871–883.

Collettini, C., and R. Sibson (2001), Normal faults, normal friction? *Geology*, *29*, 927–930.

Colgan, J., and J. Metcalf (2006), Rapid middle Miocene unroofing of the southern Ruby Mountains, Nevada, *Geol. Soc. Am. Abstracts With Programs*, *38*, 417.

Coney, P. (1980), Cordilleran metamorphic core complexes: An overview, in *Cordilleran metamorphic core complexes*, edited by M. Crittenden et al., *Geol. Soc. Am. Mem.*, *153*, 7–31.

Dalla Torre, M., W. Stern, and M. Frey (1994), Determination of white mica polytype ratios: Comparison of different XRD methods, *Clay Miner.*, *29*, 717–726.

Dallmeyer, R., A. Snoke, and E. McKee (1986), The Mesozoic-Ceneozoic tectonothermal evolution of the Ruby Mountains, East Humboldt range, Nevada: A cordilleran metamorphic core complex, *Tectonics*, *5*, 931–954, doi:10.1029/TC005i006p00931.

Damon, P., and M. Shafiqullah (2006), K-Ar ages of fault rocks along the Catalina detachment fault, Tanque Verde Ridge, Rincon Mountains, Arizona, *Arizona Geological Survey Contributed Report CR-06-A*, 18 pp., Arizona Geological Survey, Tuscon, Ariz.

Dokka, R., M. Mahaffie, and A. Snoke (1986), Thermochronologic evidence of major tectonic denudation associated with detachment faulting, northern Ruby Mountains, East Humboldt Range, Nevada, *Tectonics*, *5*, 995–1006, doi:10.1029/TC005i007p00995.

Dong, H., C. Hall, D. Peacor, and A. Halliday (1995), Mechanism of argon retention in clays revealed by laser ^{40}Ar-^{39}Ar dating, *Science*, *267*, 355–359.

Dong, H., C. Hall, A. Halliday, and D. Peacor (1997), ^{40}Ar-^{39}Ar dating of late-Caledonide (Acadian) metamorphism and cooling of K-bentonites and slates from the Welsh Basin, UK, *Earth Planet. Sci. Lett.*, *150*, 337–351.

Essene, E., and D. Peacor (1995), Clay mineral thermometry – A critical perspective, *Clay. Clay Miner.*, *43*, 540–553.

Freed, R., and D. Peacor (1989a), Diagenesis and the formation of illite-rich I/S crystals in Gulf Coast shales: A TEM study of clay separates, *J. Sediment. Petrol.*, *62*, 220–234.

Freed, R., and D. Peacor (1989b), Variability in temperature of the smectite/illite reactions in Gulf Coast sediments, *Clay Miner.*, *24*, 171–180.

Gans, P., E. Miller, J. McCarthy, and M. Ouldcott (1985), Tertiary extensional faulting and evolving ductile-brittle transition zones in the northern Snake Range and vicinity: New insights from seismic data, *Geology*, *13*, 189–193.

Gifford, L., V. Newman, D. Foster, K. Howard, and R. Donelick (2007), Quantifying Eocene and Miocene extension in the Sevier hinterland with implications for mineral and energy resources in northeastern Nevada, *Geol. Soc. Am. Abstracts With Programs*, *39*, 226.

Grathoff, G., D. Moore, R. Hay, and K. Wemmer (2001), Origin of illite in the lower Paleozoic of the Illinois Basin: Evidence for brine migration, *Geol. Soc. Amer. Bull.*, *113*, 1092–1104.

Haines, S., and B. van der Pluijm (2008), Clay quantification and Ar-Ar dating of synthetic and natural gouge, *J. Struct. Geol.*, *30*, 525–538.

Haines, S., B. van der Pluijm, M. Ikari, D. Saffer, and C. Marone (2009), Clay fabric intensity in natural and artificial fault gouges: Implications for brittle fault zone processes and sedimentary basin clay fabric evolution, *J. Geophys. Res.*, *114*, B05406, doi:10.1029/2008JB005866.

Hall, C., S. Kesler, G. Simon, and J. Fortuna (2000), Overlapping Cretaceous and Eocene alteration, Twin Creeks Carlin-type deposit, *Nevada Ceonomic Geol.*, *95*, 1739–1752.

Hames, W., and S. Bowring (1994), An empirical evaluation of the argon diffusion geometry in muscovite, *Earth Planet. Sci. Lett.*, *124*, 161–167.

Hamilton, W. (1988), Detachment faulting in the Death Valley region, California nad Nevada, *U. S. Geol. Surv. Bull.*, *1790*, 51–85.

Hayman, N., J. Knott, D. Cowan, E. Nemser, and A. Sarna-Wojicicki (2003), Quaternary low-angle slip on detachment faults in Death Valley California, *Geology*, *31*(4), 343–346.

Howard, K. (1980), Metamorphic infrastructure in the northern Ruby Mountains, Nevada, in *Cordilleran metamorphic core complexes*, edited by M. Crittenden et al., *Geol. Soc. Am. Mem.*, 153, 335–347.

Hower, J., E. Eslinger, M. Hower, and E. Perry (1976), Mechanism of burial metamorphism of argillaceous sediment: Mineralogical and chemical evidence, *Geol. Soc. Am. Bull.*, *87*, 725–737.

Huang, W., J. Longo, and D. Peaver (1993), An experimentally derived kinetic model for smectite-to-illite transformation and its use as a geothermometer, *Clay. Clay Miner.*, *41*, 162–177.

Huggett, J., and J. Cuadros (2005), Low-temperature illitization of smectite in the late Eocene and early Oligocene of the Isle of Wight (Hampshire Basin), UK, *Am. Mineral.*, *90*, 1192–1202.

Jackson, J. (1987), Active normal faulting and crustal extension, in *Continental extensional tectonics*, edited by M. Coward, J. Dewey, and P. Hancock, *Geol. Soc. Lond. Spec. Publ.*, *28*, 3–18.

Jackson, J., and N. White (1989), Normal faulting in the upper continental crust: Observations in regions of active extension, *J. Struct. Geol.*, *11*, 15–36.

John, B. (1987), Geometry and evolution of a mid-crustal extensional fault system, in *Continental Extensional Tectonics*, edited by M. Coward et al., *Geol. Soc. Spec. Publ.*, 28, 313–336.

Junfeng, J., P. Browne, and L. Yingjun (1997), Occurrence of mixed layer illite/smectite at temperature of 285°C in an active hydrothermal system and its significance, *Chin. Sci. Bull.*, *42*, 318–321.

Kim, J., H. Dong, J. Seabaugh, S. Newell, and D. Eberl (2004), Role of microbes in the smectite-to-illite transition, *Nature*, *303*, 830–832.

Kralik, M., K. Klima, and G. Riedmueller (1987), Dating fault gouges, *Nature*, *327*, 315–317.

Li, G., D. Peacor, and D. Coombs (1997), Transformation of smectite to illite in bentonite and associated sediments from Kaka Point, New Zealand: Contrasts in rate and mechanism, *Clays Clay Miner.*, *45*, 54–67.

Lonker, S., and J. Fitz Gerald (1990), Formation of coexisting 1M and 2M polytypes in illite from an active hydrothermal system, *Am. Miner.*, *75*, 1282–1290.

Lyons, J., and J. Snellenburg (1970), Dating faults, *Geol. Soc. Am. Bull.*, *82*, 1749–1752.

McGrew, A., and L. Snee (1994), ^{40}Ar/^{39}Ar thermochronologic constraints on the tectonothermal evolution of the northern East Humboldt Range metamorphic core complex, Nevada, *Tectonophysics*, *238*, 425–450.

McGrew, A., M. Peters, and J. Wright (2000) Thermobarometric constraints on the tectonothermal evolution of the East Humboldt Range metamorphic core complex, Nevada, *Geol. Soc. Am. Bull.*, *112*, 45–60.

Miller, E., T. Dumitru, R. Brown, and P. Gans (1999), Rapid Miocene slip on the Snake Range-Deep Creek fault system, east-central Nevada, *Geol. Soc. Am. Bull.*, *111*, 886–905.

Miller, J., and B. John (1999), Sedimentation patterns support low-angle normal faulting, southeastern California and western Arizona, *Geol. Soc. Am. Bull.*, *111*, 1350–1370.

Moore, D. M., and R. C. Reynolds Jr. (1997), *X-ray Diffraction and the Identification and Analysis of Clay Minerals*, Oxford Univ. Press, New York, 378 pp.

Mueller, K., and A. Snoke (1993), Progressive overprinting of normal fault systems and their role in Tertiary exhumation of the East Humboldt-Woods Hills metamorphic complex, northeast Nevada, *Tectonics*, *12*, 361–371, doi:10.1029/92TC01967.

Numelin, T., C. Marone, and E. Kirby (2007), Frictional properties of natural fault gouge from a low-angle normal fault, Panamint Valley, CA, *Tectonics*, *26*, TC2004, doi:10.1029/2005TC001916.

Peters, M. T., and S. M. Wickham (1994), Petrology of upper-amphibolite facies marbles from the East Humboldt Range, Nevada, USA: Evidence for high-temperature retrograde hydrous volatile fluxes at mid-crustal levels, *J. Petrol.*, *35*, 205–238.

Pevear, D. R. (1992), Illite age analysis, a new tool for basin thermal history analysis, in *Proceedings of the 7th International Symposium on Water-Rock Interaction*, edited by Y. K. Kharaka and A. S. Maest, Rotterdam, Netherlands, pp. 1251–1254.

Proffett, J. (1977), Cenozoic geology of the Yerrington district, Nevada, and implications for the nature of Basin and Range faulting, *Geol. Soc. Am. Bull.*, *88*, 247–266.

Pytte, A., and R. Reynolds (1989), The thermal transformation of smectite to illite, in *Thermal Histories of Sedimentary Basins: Methods and Case Histories*, edited by N. Naeser and T. McCulloh, pp. 133–140, Springer-Verlang, New York.

Reynolds, R. C., Jr. (1993), *WILDFIRE - A Computer Program for the Calculation of Three-Dimensional Powder X-ray Diffraction Patterns for Mica Polytypes and Their Disordered Variations*, Hanover, N. H.

Reynolds, R., Jr., and R. C. Reynolds III (1996), *NEWMOD-for-Windows. The Calculation of One-Dimensional X-ray Diffraction Patterns of Mixed Layered Clay Minerals*, Hanover, N. H.

Rice, J. (1992), Fault stress states, pore pressure distributions, and the weakness of the San Andreas Fault, in *Fault Mechanics and Transport Properties of Rocks: A Festschrift in Honor of W. F. Brace*, edited by B. Evans and T.-F. Wong, Academic Press, San Diego, CA, pp. 475–503.

Saffer, D., and C. Marone (2003), Comparison of smectite- and illite-rich gouge frictional properties: Application to the updip limit of the seismogenic zone along subduction megathrusts, *Earth Planet. Sci. Lett.*, *215*(1–2), 219–235.

Sandler, A., and H. Saar (2007), R >1-type illite-smectite formation at near-surface temperatures, *Clay Miner.*, *42*, 245–253.

Scholz, C. (2002), *The mechanics of earthquakes and faulting*, 471 pp., Cambridge Univ. Press, Cambridge.

Simpson, C. (1985), Deformation of granitic rocks across the brittle-ductile transition, *J. Struct. Geol.*, *7*, 503–511.

Snoke, A. (1980), Transition from infrastructure to superstructure in the Northern Ruby Mountains, Nevada, in *Cordilleran metamorphic core complexes*, edited by M. Crittenden et al., *Geol. Soc. Am. Mem.*, *153*, 287–333.

Snoke, A., and K. Howard (1984), Geology of the Ruby Mountains-East Humboldt Range, Nevada: A Cordillerian metamorphic core complex, in *Western Geological Excursions*, edited by J. Lintz, pp. 260–303, *Geol. Soc. Am. Annual Meeting Guidebook*, vol. 4, Mackay School of Mines, Reno, Nev.

Snoke, A., and A. Lush (1984), Polyphase deformation Mesozoic-Cenozoic deformational history of the

northern Ruby Mountains-East Humboldt Range, Nevada, in *Western Geological Excursions*, edited by J. Lintz, pp. 232–260, *Geol. Soc. Am. Annual Meeting Guidebook*, vol. 4, Mackay School of Mines, Reno, Nev.

Solum, J., and B. van der Pluijm (2007), Reconstructing the Snake River/Hoback Canyon segment of the Wyoming thrust belt through direct dating of fault rocks, in *Whence the Mountains? Inquiries into the Evolution of Orogenic Systems: A volume in honor of Ray Price*, *Geol. Soc. Amer. Mem.*, *433*, pp. 183–196.

Solum, J., B. van der Pluijm, and D. Peacor (2005), Neocrystallization, fabrics and age of clay minerals from an exposure of the Moab Fault, Utah, *J. Struct. Geol.*, *27*, 1563–1576.

Spencer, J. (1984), The role of tectonic denudation in the warping and uplift of low-angle normal faults, *Geology*, *12*, 95–98.

Sroden, J. (1980), Precise identification of illite/smectite interstratifications by X-ray powder diffraction, *Clays Clay Miner.*, *28*, 401–411.

Srodon, J., and D. Eberl (1984), Illite, in *Micas, Mineralogical Society of America*, edited by S. Bailey, *Rev. Mineral.*, *13*.

Stewart, J. (1983), Extensional tectonics in the Death Valley area, California: Transport of the Panamint Range structural block 80 km northward, *Geology*, *11*, 153–157.

Tembe, S., D. Lockner, J. Solum, C. Morrow, T.-F. Wong, and D. Moore (2006), Frictional strength of cuttings from the SAFOD drill hole: Phases 1 and 2, *Geophys. Res. Lett.*, *33*, L23307, doi:10.1029/2006GL027626.

Tembe, S., D. Lockner, and T.-F. Wong (2009), Constraints on the stress state of the San Andreas Fault with analysis based on core and cuttings from the San Andreas Fault Obseratory at Depth (SAFOD) drilling phases 1 and 2, *J. Geophys. Res.*, *114*, B11401, doi:10.1029/2008JB005883.

Vanderhaeghe, O., C. Teyssier, I. McDougall, and W. Dunlap (2003), Cooling and exhumation of the Shuswap Metamorphic Core Complex constrained by $^{40}Ar/^{39}Ar$ thermochronology, *Geol. Soc. Am. Bull.*, *115*(2), 200–216.

van der Pluijm, B., C. Hall, P. Vrolijk, D. Pevear, and M. Covey (2001), The dating of shallow faults in the Earth's crust, *Nature*, *412*, 172–175.

van der Pluijm, B., P. Vrolijk, D. Pevear, C. Hall, and J. Solum (2006), Fault dating in the Canadian Rocky Mountains: Evidence for late Cretaceous and early Eocene orogenic pulses, *Geology*, *34*, 837–840.

Velde, B. (1965), Experimental determination of muscovite polymorph stabilities, *Am. Mineral.*, *50*, 436–449.

Voll, G. (1976), Recrystallization of quartz, biotite and feldspars from Erstfeld to the Leventina Nappe, Swiss Alps, and its geological significance, *Schweiz. Mineral. Petrogr. Mittl.*, *56*, 641–647.

Vrolijk, P., and B. van der Pluijm (1999), Clay Gouge, *J. Struct. Geol.*, *21*, 1039–1048.

Wernicke, B. (1995), Low-angle normal faults and seismicity: A review, *J. Geophys. Res.*, *100*, 20,159–20,174, doi:10.1029/95JB01911.

Wernicke, B., and G. Axen (1988), On the role of isostasy in the evolution of low-angle normal fault systems, *Geology*, *16*, 848–851.

Whitney, G. (1990), Role of water in the smectite to illite reaction, *Clays Clay Miner.*, *38*, 343–350.

Wong, M., and P. Gans (2003), Tectonic implications of early Miocene extensional unroofing of the Sierra Mazatán metamorphic core complex, Sonora, Mexico, *Geology*, *31*(11), 953–956.

Wong, M., and P. Gans (2008), Geologic, structural and thermochronologic constraints on the tectonic evolution of the Sierra Mazatán core complex, Sonora, Mexico: Insights into metamorphic core complex formation, *Tectonics*, *27*, TC4013, doi:10.1029/2007TC002173.

Ylagan, R., C. Kim, D. Pevear, and P. Vrolijk (2002), Illite polytype quantification for accurate K-Ar determination, *Amer. Mineral.*, *87*, 1536–1545.

Yoder, H., and H. Eugster (1955), Synthetic and natural muscovites, *Geochem. Cosmochem. Acta*, *8*, 225–280.

S. H. Haines, Department of Geosciences, Pennsylvania State University, 510 Deike Bldg., University Park, PA 16801, USA. (shh13@psu.edu)

B. A. van der Pluijm, Department of Geological Sciences, University of Michigan, Ann Arbor, MI 48109, USA.